An engineered TGF-β monomer that functions as a dominant negative to block TGF-β signaling

Kim, Sun Kyung; Barron, Lindsey; Hinck, Cynthia S.; Petrunak, Elyse M.; Cano, Kristin E.; Thangirala, Avinash; Iskra, Brian; Brothers, Molly; Vonberg, Machell; Leal, Belinda; Richter, Blair; Kodali, Ravindra; Taylor, Alex B.; Du, Shoucheng; Barnes, Christopher O.; Sulea, Traian; Calero, Guillermo; Hart, P. John; Hart, Matthew J.; Demeler, Borries; Hinck, Andrew P.

Publisher's version / Version de l'éditeur:
https://doi.org/10.1074/jbc.M116.768754
The Journal of Biological Chemistry, 2017-02-22

JBC Papers in Press. Published on February 22, 2017 as Manuscript M116.768754
The latest version is at http://www.jbc.org/cgi/doi/10.1074/jbc.M116.768754

An Engineered TGF-β Monomer that Functions as a Dominant Negative to Block TGF-β signaling

Sun Kyung Kim, Lindsey Barron, Cynthia S. Hinck, Elyse M. Petrunak, Kristin E. Cano, Avinash Thangirala, Brian Iskra, Molly Brothers, Machell Vonberg, Belinda Leal, Blair Richter, Ravindra Kodali, Alexander B. Taylor, Shoucheng Du, Christopher O. Barnes, Traian Sulea, Guillermo Calero, P. John Hart, Matthew J. Hart, Borries Demeler, and Andrew P. Hinck

From the Department of Structural Biology, University of Pittsburgh School of Medicine, Pittsburgh, PA 15260 U.S.A, the Department of Biochemistry, the Department of Cell and Structural Biology, and Center for Innovative Drug Discovery, University of Texas Health Science Center at San Antonio, San Antonio, TX 78229-3900 U.S.A., and the National Research Council, Human Health Therapeutics Portfolio, Montréal, Quebec, H4P2R2 Canada

Running title: Engineered TGF-β Monomer that Blocks TGF-β Signaling

To whom correspondence should be addressed: Prof. Andrew P. Hinck, Department of Structural Biology, University of Pittsburgh School of Medicine, Biomedical Science Tower 3, Room 1035, 3501 Fifth Avenue, Pittsburgh, PA 15260, U.S.A, Telephone: (412) 648-8533, FAX: (412) 648-9008, E-mail: ahinck@pitt.edu

Keywords: transforming growth factor beta (TGF-β), dominant negative, protein engineering, inhibitor, cell signaling, cancer, fibrosis

ABSTRACT

The transforming growth factor beta isoforms, TGF-β1, -β2, and –β3 are small secreted homodimeric signaling proteins with essential roles in regulating the adaptive immune system and maintaining the extracellular matrix. However, dysregulation of the TGF-β pathway is responsible for promoting the progression of several human diseases, including cancer and fibrosis. In spite of the known importance of TGF-βs in promoting disease progression, no inhibitors have been approved for use in humans. Herein, we describe an engineered TGF-β monomer, lacking the heel helix, a structural motif essential for binding the TGF-β type I receptor, TβRI, but dispensible for binding the other receptor required for TGF-β signaling, the TGF-β type II receptor, TβRII, as an alternative therapeutic modality for blocking TGF-β signaling in humans. As shown through binding studies and crystallography, the engineered monomer retained the same overall structure of native TGF-β monomers and bound TβRII in an identical manner. Cell-based luciferase assays showed that the engineered monomer functioned as a dominant negative to inhibit TGF-β signaling with a K_i of 20 – 70 nM. Investigation of the mechanism showed that the high affinity of the engineered monomer for TβRII, coupled with its reduced ability to non-covalently dimerize and its inability to bind and recruit TβRI, enabled it to bind endogenous TβRII, but prevented it from binding and recruiting TβRI to form a signaling complex. Such engineered monomers provide a new avenue to probe and manipulate TGF-β signaling, and may inform similar modifications of other TGF-β family members.

The transforming growth factor beta isoforms, TGF-β1, -β2, and -β3, are small secreted signaling proteins. Their overall structures are similar and consist of two cystine-knotted monomers tethered together by a single inter-chain disulfide bond (5). They coordinate wound healing, modulate immune cell function, maintain the extracellular matrix, and regulate epithelial and

endothelial cell growth and differentiation (6). The TGF-βs are synthesized as pre-pro proteins and after maturation, secretion, and release from their pro-domains (7), the mature homodimeric growth factors (GFs) bind and bring together two single-pass transmembrane receptors, known as TβRI and TβRII, to form the signaling-competent $T\beta RI_2$-$T\beta RII_2$ heterotetramer (8,9). TGF-β GFs assemble $T\beta RI_2$-$T\beta RII_2$ heterotetramer in a sequential manner, first by binding TβRII followed by recruitment of TβRI (10,11). The stepwise assembly of TβRII and TβRI into a heterotetramer is driven by binding of TβRI to a composite TGF-β:TβRII interface (12,13) (Fig. 1*A*).

The disruption or dysregulation of the TGF-β pathway is responsible for several human diseases. These include connective tissue disorders, such as Marfan's disease and Loeys-Dietz syndrome, which are caused by increased or decreased signaling due to mutations in the matrix protein fibrillin-1 or TβRII, respectively (2,14). The dysregulation of the pathway is also responsible for fibrotic disorders (1) and soft tissue cancers (4). The fibrotic disorders are a result of hyperactive TGF-β signaling following tissue injury or disease progression that leads to the accumulation of extracellular matrix proteins. TGF-β's role in cancer is complex, with loss of its potent growth inhibitory activity being responsible for cancer initiation (15), and excessive TGF-β signaling, in the context of growth refractory advanced cancers, potently stimulating cancer progression and metastasis (4).

TGF-β's disease promoting activities, together with animal studies that have demonstrated beneficial effects of inhibiting TGF-β in models of cancer and fibrosis (16-23), have made them important targets for the development of inhibitors. However, in spite of clinical trials ongoing for nearly two decades using receptor kinase inhibitors, neutralizing antibodies, and other approaches, no TGF-β inhibitors have been approved for clinical use in humans (24,25). One of the main challenges involves finding the correct dosing and pharmacodynamics for the particular disease to enable an effective therapeutic response, but sparing or minimally impacting TGF-β signaling, or other signaling pathways, in normal cells and tissues. TGF-β kinase inhibitors have posed some challenges in this respect as they have significant inhibitory activity against other type I receptors of the TGF-β superfamily, as well as other related kinases (26-28), and may further lead to rapid development of resistance (29). Pan-isoform TGF-β neutralizing antibodies, such as Sanofi's humanized mouse mononclonal antibody, GC1008, are specific, though tissue residence times are long and some concerning side effects, such as keratoacanthoma and squamous cell carcinoma, have been reported in clinical trials (30).

Thus, alternative approaches are needed to target the TGF-β pathway. The objective of this study was to investigate whether it might be possible to design an engineered TGF-β GF that functioned as a dominant negative to potently and specifically inhibit TGF-β signaling. This approach offers several potential advantages over existing therapies. Relative to kinase inhibitors, engineered GFs would be expected to have much higher specificity, especially if they function by binding and blocking TβRII, which is known to only bind and transduce signals for TGF-β1, -β2, and -β3, but not other TGF-β family GFs (5,31). Another potential advantage over kinase inhibitors is increased bioavailability, since unlike the kinase inhibitors, engineered GFs would not have to cross the plasma membrane to reach their target. Relative to monoclonal antibodies, the engineered GFs, because of their smaller size, would be expected to have shorter tissue lifetimes, which would limit sustained inhibition in normal cells and tissues and may alleviate undesirable side effects. The smaller size of engineered GFs may also lead to improved penetration of diseased tissues, particularly solid tumors, relative to 150 kDa monoclonal antibody molecules (32,33). Engineered ligands have been successfully used to target other signaling pathways, such as the VEGF pathway (34), and thus represent a largely undeveloped, but potentially very effective therapeutic modality for treating disease.

Through previous studies, monomeric forms of TGF-β1 and TGF-β3, formed by substituting the cysteine residue that forms the inter-chain disulfide to serine (C77S), were shown to have diminished signaling activity compared to their disulfide-linked counterparts, but nonetheless were still quite potent, with EC_{50}s for stimulation of TGF-β reporter gene activity in the range of 100 pM (11,35). Amatayakul-Chantler and co-

workers (35), and later Zúñiga and co-workers (11), suggested this residual activity might arise from assembly of a dimeric complex of a GF homodimer and two bound TβRIs and two bound TβRIIs, but without the disulfide linkage between the GF monomers. This model was attractive for two reasons – first, structures of the TGF-βs show there are in fact extensive hydrophobic contacts between the TGF-β monomers that could promote non-covalent self-association of the monomers (Fig. 1*B*) (36,37) – once formed, these non-covalent dimers would be stabilized as the receptors bind, since crystal structures show that at least one them, TβRI, binds by straddling the TGF-β homodimer interface (Fig. 1*A*, *C*) (12,13).

The objective of this study was to design an engineered TGF-β monomer that still retained its full capacity to bind the high affinity TGF-β receptor, TβRII, but was fully impaired in its ability to bind and recruit TβRI. This type of engineered monomer would be expected to function as a dominant negative, and thus inhibit TGF-β signaling, since it would bind and thus occupy cell surface TβRII, but in turn be unable to recruit TβRI to form a signaling complex. The results presented here document the generation of such an engineered monomer and demonstrate that such monomers function as potent inhibitors of TGF-β signaling in cultured cells. The results further show that unlike dimeric TGF-βs, as well as their C77S monomeric counterparts, engineered monomers are highly soluble. These properties, together with the high intrinsic specificity of TGF-βs for TβRII, should engender this novel inhibitor with favorable properties for treating human diseases, such as Marfan's disease, fibrotic disorders, and soft tissue cancers that are driven by excessive TGF-β signaling.

RESULTS

Design of engineered mini monomeric TGF-β (mmTGF-β) - The structures of the TGF-β receptor complexes (12,13), as well as accompanying binding and crosslinking studies with TGF-β3 C77S (11,12,38), suggested that the signaling capacity of monomeric TGF-βs (TGF-β1 C77S or mTGF-β1 and TGF-β3 C77S or mTGF-β3) arise from their ability to non-covalently dimerize and in turn bind their receptors. (Fig. 1*A*, *C*). This led to our hypothesis that it should be possible to diminish or completely eliminate receptor complex assembly with monomeric TGF-βs by removing or altering residues responsible for dimer formation and binding of TβRI. The structural motif that likely contributes the greatest to self-association of the monomers is the 'heel' α-helix, α-helix 3 (Fig. 1*A*). This helix is highly amphiphatic and has numerous hydrophobic interactions with residues that line the 'palm' of the opposing monomer (Fig. 1*B*). This helix also forms a large portion of the binding surface for TβRI (Fig. 1*C*). Thus, it was hypothesized that elimination of α-helix 3 should interfere with both self-association of the monomers and binding of TβRI, but should not impair TβRII binding as this occurs through the ligand fingertips far away from α-helix 3 (Fig. 1*A*).

To evaluate this hypothesis, bacterial expression constructs were generated for TGF-β1, TGF-β2, and TGF-β3 in which residues 52 – 71 were eliminated and Cys77 was substituted with serine. This corresponds to deletion of all of α-helix 3, as well as five flanking residues on the N-terminal end and three flanking residues on the C-terminal end (Fig. 1*D*). The length of the deletion was chosen so as to leave a sufficient number of residues between the last residue of β-strand 4 (G48) and the first residue of β-strand 5 (C77/S77) to form an unconstrained loop that bridges β-strands 4 and 5. Though a secondary consideration, either two (TGF-β2) or three (TGF-β1 and -β3) of the loop forming residues were also substituted so as to increase the net overall charge at pH 7.0 for the full-length TGF-β1, -β2, and -β3 monomers from -0.9, +1.1, and +4.4 to -3.1, +3.9, and +6.1 for the constructs in which α-helix 3 was deleted (Fig. 1*D*). The rationale for this was that the solubility of the monomers, which like the homodimers are poor from pH 4.5 to 9.5 (see Fig. 4*A-B* below), might be improved by both removing hydrophobic α-helix 3 and by artificially increasing the net charge at pH 7.0.

Isolation and physical characterization of mmTGF-β2 - The TGF-β1, -β2, and –β3 'mini monomers' described above, designated mmTGF-β1, mmTGF-β2, and mmTGF-β3, were expressed in *E. coli* and accumulated in the form of insoluble inclusion bodies. The inclusion bodies were isolated and after reconstitution and purification in denaturant, the mini monomers were renatured by dilution into CHAPS-containing buffer at pH 9.0

as previously described (39). The folding of the mini monomers differed greatly: a large portion of the mmTGF-β2 remained soluble during the folding and yielded large amounts of monomeric protein after purification by cation exchange chromatography, while only a small amount of mmTGF-β1 and mmTGF-β3 remained soluble during the folding and either no monomeric protein (TGF-β1) or a very small amount of monomeric protein (TGF-β3) was obtained after purification by cation exchange chromatography. This pattern mirrors that previously observed for the folding of TGF-β homodimers from full-length wild type monomers (39) and likely reflects differences in the intrinsic propensity of the monomers to properly form the four intramolecular disulfides characteristic of each monomer.

Though mmTGF-β2 was the least desired variant, due to expected low intrinsic affinity for binding TβRII, this was nonetheless considered something that could be relatively easily addressed. This follows based on our prior studies which demonstrated that substitution of the three residues in TGF-β2's interface with TβRII that differ from those in TGF-β1 and TGF-β3 was sufficient to engender TGF-β2 with the ability to bind TβRII with high affinity (40,41).

To determine if mmTGF-β2 was suitable for further development in the manner described above, it was characterized in terms of its folding, solubility, and receptor binding properties. To assess folding, a ^{15}N-labeled sample of mmTGF-β2 was prepared and examined by recording a two-dimensional ^{1}H-^{15}N shift correlation spectrum (Fig. 2*A*). This revealed a highly dispersed spectrum characteristic of natively folded protein. The spectrum could be fully assigned and analysis of the assigned chemical shifts to identify secondary structure propensities showed that the protein had the expected secondary structure, particularly in the palm region formed by the cystine knot and the finger region where TβRII binds (Supplemental Fig. S2*A*). This analysis further showed that the newly created loop between residues 47 - 56 had near zero probability of forming either an α-helix or β-strand, suggesting that it is likely flexible as would be expected for a loop of this length connecting two antiparallel β-strands. This was directly confirmed by an analysis of backbone ^{15}N T_2 values. These provide information about motions on fast (ns-ps) and intermediate (μs-ms) timescales and were significantly elevated in the region corresponding to the newly created loop relative to the other parts of the protein (Supplemental Fig. S2*B*), which except for the N-terminus and the short loop connecting α-helix 1 and β-strand 1, are expected to be structurally well-ordered.

To directly examine the three-dimensional structure, mmTGF-β2 was crystallized and its structure was determined to a resolution of 1.8 Å using molecular replacement (Table 1). The overall fold of mmTGF-β2 was shown to be highly similar to that previously determined for TGF-β2, with the exception of the newly created loop, which was shown to take the place of α-helix 3 as anticipated (Fig. 2*B*). Superposition of the mmTGF-β2 with the monomer from the structure of TGF-β2 shows that there is a systematic displacement of up to about 1.5 Å of the finger region of mmTGF-β2 relative to TGF-β2. Such differences appear to be a result of bending of the monomer near the center of the finger region, not a change in the structure of the finger region, as superimposition of the fingers alone show that they correspond closely, with a backbone RMSD of under 0.2 Å and similar orientations of the sidechains of several residues that pack and stabilize the fingers (Fig. 2*D*). Such bending is also supported by an overlay of the two molecules of mmTGF-β2 present in the crystallographic asymmetric unit, which also exhibit a smaller but still noticeable displacement of the finger regions relative to one another (Fig. 2*C*). Consistent with the NMR analysis, not only was the electron density noticeably weaker in the region corresponding to the newly created loop, but also it was shown to adopt different orientations for the two molecules from the asymmetric unit (Fig. 2*C*).

The similar folding of mmTGF-β2 relative to TGF-β2, especially in the TβRII-binding finger region, suggested that it would also bind TβRII in a similar manner. To evaluate this, surface plasmon resonance (SPR) experiments were performed in which the same concentration series of TβRII was injected over TGF-β2 and mmTGF-β2 immobilized on separate flow cells (Figure 3*A*, *B*). Though it was not possible to quantitate affinity due to weak binding, the sensorgrams nonetheless showed similar shapes and

concentration dependence. These sensorgrams show that mmTGF-β2 binds TβRII weakly, consistent with earlier reports (40), and that it does so in a manner qualitatively similar to TGF-β2.

The solubility of mmTGF-β2 appeared to be significantly better than that of TGF-β2 and the full-length TGF-β2 monomer, mTGF-β2, as samples of the former could be readily prepared at concentrations of 2 – 3 mg mL^{-1} without noticeable precipitation at pH 7.0, whereas samples of the latter two proteins were completely precipitated under these same conditions. To quantitate solubility, TGF-β2, mTGF-β2, and mmTGF-β2 were prepared as concentrated stocks in 100 mM acetic acid (pH 2.9) where they were readily soluble and then diluted into PBS at pH 7.4. The light scattering at 340 nM was measured to assess precipitation, and then the samples were centrifuged and the absorbance at 280 nM was measured to assess the protein concentration. This demonstrated that TGF-β2 and mTGF-β2 were both effectively insoluble at neutral pH over the entire concentration range evaluated (7 – 100 μM) (Fig. 4*A-B*). This is consistent with the known poor solubility of the TGF-β homodimers (42), but shows that this property also extends to full-length monomeric TGF-βs. The mini monomeric TGF-β2, mmTGF-β2, in contrast, exhibited modest light scattering and a corresponding modest reduction in the amount of soluble protein relative to that expected when the protein concentration was 40 μM or higher, indicating that indeed mmTGF-β2 was reasonably soluble at neutral pH, although not perfectly so. This was reflected in NMR spectra which showed that although 100 – 200 μM ^{15}N mmTGF-β2 samples could be readily prepared, the spectrum was nonetheless poor, with the only detectable signals arising from residues in the flexible parts of the protein, namely the N-terminus, the exposed loop between α-helix 1 and β-strand 1, and the newly created loop between β-strands 4 and 5. The fact that signals could only be detected from the flexible parts of the protein suggested that mmTGF-β2 forms large soluble aggregates under these conditions. Through trial and error, it was found that these soluble aggregates could be eliminated by addition of the zwitterionic detergent CHAPS, with the majority of the NMR signals appearing at concentration of 5 mM CHAPS and all of the NMR signals appearing at 10 mM CHAPS. Thus, all NMR spectra, including that shown in Fig. 2*A*, were recorded in the presence of 10 mM CHAPS.

Isolation and physical characterization of mmTGF-β2-7M - The results presented above show that while mmTGF-β2 is natively folded, it nonetheless possesses low intrinsic affinity for binding TβRII. In order to confer mmTGF-β2 with the ability to bind TβRII with high affinity comparable to that of TGF-β1 and TGF-β3, the three residues in mouse TGF-β2 shown previously to differ in the interface with TβRII, K25, I92, and N94 (41,43), were substituted with the corresponding residues from TGF-β1 and -β3, R25, V92, and R94 (Fig. 1*E, F*). In previous studies, substitution of these three residues was shown to be sufficient to confer TGF-β2 with a TβRII binding affinity comparable to TGF-β1 and TGF-β3 (40,41). In spite of this, four additional residues peripheral to the TβRII binding site that differed in TGF-β2 relative to TGF-β1 were also substituted with the corresponding residues from TGF-β1 (R26K, L89V, T95K, I98V) (Fig. 1*E*, *F*). Though previous results suggested this was not strictly necessary, it was nonetheless done to ensure that the precise orientation of residues in mmTGF-β2's binding site for TβRII matched as closely as possible with that in the high affinity TGF-β isoforms, TGF-β1 and TGF-β3. The resulting construct bearing these seven amino acid substitutions, designated mmTGF-β2-7M (Fig. 1*E*, Supplemental Fig. S1, Supplemental Table S1), was expressed in *E. coli* in the form of insolulble inclusion bodies. As with mmTGF-β2, most of the protein remained in solution after reconstitution and dilution into native folding buffer, and large amounts of homogenous monomer could be isolated (4 – 5 mg per liter of *E. coli* culture medium).

The folding and homogeneity of the isolated mmTGF-β2-7M was evaluated by NMR, and as with mmTGF-β2, the protein was found to have the expected number of signals in a 2D ^{1}H-^{15}N shift correlation spectrum (Fig. 5*A*) as well as secondary structure, as determined by an analysis of the NMR secondary shifts (Supplemental Fig. S3*A*). The solubility of mmTGF-β2-7M was evaluated as before, and as shown, its behavior was comparable or perhaps slightly better than that of mmTGF-β2 (Fig. 4*C*, *D*). This slight improvement in the macroscopic solubility did not

however change the microscopic solubility as NMR analysis showed that it was still necessary to include 10 mM CHAPS in the sample buffer in order to detect signals from all of the backbone amide resonances in the protein.

The three-dimensional structure of mmTGF-β2-7M was determined by crystallography to a resolution of 2.75 Å (Table 1), and as before the overall fold was preserved relative to TGF-β2, with the only difference being a slight hinge bending of the monomer as described for mmTGF-β2 (Fig. 5*B*, *C*). The increase in the ^{15}N T_2 relaxation times in the region corresponding to the newly formed loop in mmTGF-β2-7M was comparable to that in mmTGF-β2 (Supplemental Fig. S3*B*). This suggested that the missing density in the region corresponding to the newly formed loop in mmTGF-β2-7M, which among the three molecules in the asymmetric unit was observed for part of chain A and most of chain C, was not due to increased dynamics, but other factors, most likely the lower resolution of the mmTGF-β2-7M structure compared to the mmTGF-β2 structure (Table 1).

To determine whether mmTGF-β2-7M bound TβRII with high affinity, variants of mmTGF-β2-7M and TGF-β3 were produced bearing an N-terminal avitag, and after biotinylation and immobilization onto a streptavidin-coated SPR sensor, their binding affinity for TβRII was measured by performing kinetic SPR experiments (Fig. 3*C*, *D*). The sensorgrams obtained differed greatly from that previously obtained for mmTGF-β2 and TGF-β2, in that they exhibited a clear pattern of saturation. The sensorgrams were furthermore shown to have similar shapes as well as fitted parameters, including K_D values (Table 2), which were within experimental error of one another and consistent, although on the high end, of K_D values reported earlier for TβRII binding to TGF-β1 and TGF-β3 (38,40,41).

To determine if the interactions that enabled high affinity TβRII binding were preserved in mmTGF-β2-7M compared to TGF-β1 and TGF-β3, the mmTGF-β2-7M:TβRII complex was crystallized and its structure was determined to a resolution of 1.88 Å (Table1). The overall structure of the mmTGF-β2-7M:TβRII complex is shown to be very similar to that of one of the TβRII-bound monomers from the structure of the TGF-β3:TβRII:TβRI complex, with TβRII bound to the mmTGF-β2-7M fingertips in a manner that is essentially indistinguishable from that of TGF-β3 (Fig. 5*D*). The interactions known to contribute most significantly to high affinity binding are furthermore shown to be fully preserved in the mmTGF-β2-7M:TβRII complex relative to TGF-β1:TβRII and TGF-β3:TβRII complexes that have been previously determined (the TGF-β3:TβRII complex determined to 1.8 Å (43) is shown as this is the highest resolution structure determined to date) (Fig. 5*E*). This includes the packing of I53 from TβRII in the hydrophobic pocket between the TGF-β fingers, and the hydrogen-bonded ion pairs formed between TGF-β R25 and R94 on the tips of the loops connecting fingers 1/2 and 3/4, respectively, and the carboxylate groups of E119 and D32 on TβRII (Fig. 5*E*).

Inhibitory activity of mmTGF-β2-7M and the underlying mechanism - The results presented above show that mmTGF-β2-7M possesses one of the essential attributes required to function as a dominant negative inhibitor of TGF-β signaling, that is the ability to bind TβRII with high affinity, comparable to that of TGF-β1 and TGF-β3. To directly assess whether mmTGF-β2-7M might signal, and if not, whether it might function as an inhibitor, TGF-β signaling was assessed by treating HEK293 cells stably transfected with a TGF-β luciferase reporter under the control of a $CAGA_{12}$ promoter (44) with increasing concentrations of TGF-βs. The results showed that dimeric TGF-β1 (TGF-β1) and full-length monomeric TGF-β3 (mTGF-β3) resulted in a sigmoidal increase in the luciferase response, with concentrations of roughly 10 pM TGF-β1 and 100 pM mTGF-β3 leading to no further increase in the measured luciferase response. This is consistent with earlier reports which showed that (full-length) monomeric TGF-β1 and -β3 were 5 – 15 fold less potent than their dimeric counterparts (11,35). The normalized luciferase responses could be readily fitted to a standard model for ligand-dependent activation and yielded EC_{50} values of 12.4 ± 1.5 pM for TGF-β1 and 182 ± 16 pM for mTGF-β3. The values for TGF-β1 and mTGF-β3 are in close accord with the values previously reported by Amatayakul-Chantler for TGF-β1 (35) and by

Zúñiga and coworkers for mTGF-β3 (11). The potent sub-nanomolar signaling activity observed for TGF-β1 and mTGF-β3 stands in contrast to that of mmTGF-β2-7M, which had no detectable signaling activity at the concentration that led to a saturating response for mTGF-β3 (ca. 200 pM) or at concentrations that were up to four orders of magnitude higher (Fig 6*A*). Thus, mmTGF-β2-7M was either completely devoid of signaling activity, or it possessed signaling activity, but with a potency more than a 10000-fold less than that of mTGF-β3.

To further investigate the properties of mmTGF-β2-7M, a competition experiment was performed in which the same HEK293 luciferase reporter cell line was stimulated with a constant sub-EC_{50} concentration of dimeric TGF-β1 (8.0 pM) and increasing concentrations of mTGF-β3 or mmTGF-β2-7M. The results showed that mTGF-β3 further stimulated signaling with a midpoint concentration similar to that of mTGF-β3 alone (Fig. 6*B*). The fitted EC_{50} values confirm this, with an EC_{50} of 182 ± 16 pM for the data shown in Fig. 6*A* and EC_{50} of 194 ± 36 pM for the data shown in Fig. 6*B*. The behavior of mmTGF-β2-7M was very different, with no detectable change in the signaling activity when added up to concentrations of 10 nM, but with a sharp decrease to no detectable signaling activity when the concentration was increased to 100 nM (Fig. 6*B*). This shows that mmTGF-β2-7M indeed possesses no signaling activity and that it can function to completely block and inhibit TGF-β signaling. The normalized luciferase responses could be readily fitted to a standard model for ligand-dependent inhibition and yielded an IC_{50} value of 68 ± 7 nM. Similar experiments showed that mmTGF-β2-7M also functioned as a potent competitive inhibitor against the other TGF-β isoforms, TGF-β2 and TGF-β3, with measured IC_{50} values (TGF-β2 IC_{50} 19 ± 3 nM and TGF-β3 IC_{50} 21 ± 8 nM) within a factor of 2 -3 of that measured for TGF-β1 (Supplement Fig. S4*A*, *B*). These IC_{50} values are on the lower end of the range of affinities that have been reported for binding of the high affinity TGF-β isoforms to TβRII, including mmTGF-β2-7M reported here (Table 2). This suggests that mmTGF-β2-7M functions to inhibit TGF-β signaling in the manner anticipated, that is by binding to and blocking endogenous TβRII. The fact that the measured potency is greater than the greatest affinity previously reported for TGF-β1 and TGF-β3 binding to TβRII (140 nM) (13), suggest that other factors, such as non-specific association of mmTGF-β2-7M with the plasma membrane, may serve to potentiate its inhibitory activity.

The finding that mmTGF-β2-7M possesses no apparent signaling activity, and in fact functions as low nM inhibitor of TGF-β signaling, suggests that the elimination of α-helix 3 in fact diminished non-covalent association of the monomers and greatly attenuated or abrogated TβRI binding. To assess this directly, SPR experiments were performed to determine if mmTGF-β2-7M could recruit TβRI in the presence of TβRII. To accomplish this, increasing concentrations of TβRI, as well as the same concentration series of TβRI in the presence of near-saturating amount of TβRII (2 μM) were injected over the same TGF-β3 and mmTGF-β2-7M SPR chip surfaces used for the TβRII binding measurements described above. This showed that TβRI alone binding is negligible to both TGF-β3 and mmTGF-β2-7M (Figures 3*E*, *F*), but unlike TGF-β3, TβRII-bound mmTGF-β2-7M is unable to recruit TβRI (Figures 3*G*, *H*). This is consistent with the earlier result reported by Huang and co-workers that TβRII-bound mTGF-β3 was significantly or completely impaired in terms of its ability to bind and recruit TβRI (38). This also provides further evidence that TβRII-bound TGF-β monomers are incapable of binding and recruiting TβRI, but because the mmTGF-β2-7M was immobilized on the surface of the sensor, it alone does not provide any insight as to whether mmTGF-β2-7M might be capable of non-covalently dimerizing and binding and recruiting TβRI.

To address these questions directly, two solution based techniques were used, analytical ultracentrifugation (AUC) and time-resolved fluorescence resonance energy transfer (TR-FRET). The AUC experiments were performed by measuring the total UV absorbance at 280 nm as a function of the radial position and time as mTGF-β3, mmTGF-β2, and mmTGF-β2-7M were sedimented under acidic conditions (pH 3.8) where the monomers are fully soluble. The AUC data revealed parabolically-shaped van Holde-Weischet sedimentation coefficient distribution

plots for all three monomers (not shown), consistent with each undergoing reversible self-association to form a dimer or other higher order oligomer. To determine more precisely which species might be present in solution, the data was fitted to the simplest model possible, a discrete monomer-dimer equilibrium, using finite element analysis as described in *Experimental Procedures*. The fitting procedure resulted in near-perfect fits for all three monomers to the simple monomer-dimer model, as shown by a) the close overlays between the fitted curves (red) with the raw data, after the time- and radially invariant noise was removed (black) and b) the absence of any systemic deviations in the residuals (Supplemental Figs. S5 – S7). The fitted parameters further showed that K_D for self-association was one order of magnitude greater for mTGF-β3 compared to mmTGF-β2 and mmTGF-β2-7M. Thus, the removal of the heel helix, α3, does diminish self-association of the monomers to form dimers, but it does not completely abrogate dimer formation.

TR-FRET was used to assess the ability of dimeric and monomeric TGF-βs to bind and bring TβRI and TβRII together. This was accomplished by generating differentially tagged forms of TβRII and TβRI and in turn binding to these tags with proteins labeled with fluorescent donors and acceptors: TβRII was tagged with a C-terminal histag and was bound by a terbium cryptate-labeled Anti-His monoclonal antibody fluorescent donor and TβRI was tagged with an N-terminal avitag, which after enzymatic biotinylation, was bound to a dye-labeled (XL-665) streptavidin fluorescent acceptor (Fig. 7*A*). The addition of TGF-β to the tagged receptors brings them together and leads to a large increase in the ΔF value, which is defined as the ratio of the acceptor and donor emission fluorescent intensities. The TR-FRET assay is demonstrated by the data presented in Supplemental Figure S8 and was used here to compare the ability of the TGF-β3 full-length monomer, mTGF-β3, and the TGF-β2 mini monomer that binds TβRII with high affinity, mmTGF-β2-7M, to bind and bring TβRI and TβRII together. The TR-FRET signal for mTGF-β3 was shown to be comparable to that of TGF-β3 and this did not depend on whether the TGF-β concentration was 100 nM or 250 nM (Fig. 7*B*). The TR-FRET signal of mmTGF-β2-7M was, in contrast, within the error limits of the buffer control and this also did not depend on the TGF-β concentration (Fig. 7*B*). These results demonstrate that under these conditions, mTGF-β3 retains full capacity to assemble a non-covalent dimeric complex with TβRI and TβRII, while under these same conditions, mmTGF-β2-7M has no capacity to do so. These results, together with the AUC results, suggest that the removal of the heel helix had the effects anticipated: its removal appears to have reduced, although not eliminated dimer formation, and even though dimers are still formed, they are evidently unable to bind and recruit TβRI.

DISCUSSION

The TGF-βs are responsible for promoting the progression of numerous human diseases (1-4), yet in spite of nearly two decades of preclinical studies and clinical trials, no inhibitors have been approved for use in humans. The results presented here demonstrate that an engineered TGF-β monomer, lacking Cys77 and the heel α-helix (α3), functions to potently block and inhibit signaling of the TGF-β1, -β2, and –β3 with IC_{50}s in the range of 20 – 70 nM (Fig. 6B, Supplemental Fig. S4). This novel inhibitor has several attributes that may overcome limitations that have been encountered with other classes of inhibitors – for example, the natural high specificity of TGF-β, and thus the inhibitor, for TβRII may engender it with much greater specificity, and thus fewer undesirable side effects, compared to the much more promiscuous TGF-β kinase inhibitors. The small size of the inhibitor (ca. 10 kDa) may further engender it with a much greater ability to penetrate tumors and other dense tissues where the TGF-βs drive disease progression, a distinct advantage compared to IgG antibodies, which are much larger (ca. 150 kDa) and tend to occupy only the vascular and interstitial space of well-perfused organs (32,33). The other advantages of this novel inhibitor include its high intrinsic stability, owing to the four intramolecular disulfide bonds that tie the four fingers together, and the fact that it is highly soluble in water at neutral pH, unlike native TGF-β dimers or full-length TGF-β monomers.

The structures of TGF-β receptor complexes, together with the previous published chemical crosslinking data, suggested that the potent signaling activity of TGF-β1 C77S and TGF-β3 C77S was due to the ability of the monomers to non-covalently dimerize and in turn

assemble a $(T\beta RI:T\beta RII)_2$ heterotetramer. The results presented here, namely the AUC experiments which were used to assess non-covalent dimer formation, and the TR-FRET experiments which were used to assess assembly of complexes with TβRI and TβRII, provided further evidence for this. The AUC data showed that full length monomeric TGF-β3, mTGF-β3, self-associates to form dimers with a dimerization constant of 4.1 μM (Table 3). The TR-FRET data showed that at a concentration of 0.1 or 0.25 μM and in the presence of comparable concentrations of the TβRI and TβRII ectodomains, mTGF-β3 assembles TβRI:TβRII complexes to the same extent as dimeric TGF-β3 (Fig. 7*B*). That this occurs, even under conditions where the mTGF-β3 concentrations (0.1 – 0.25 μM, Fig. 7*B*) were more than an order of magnitude below the K_D for self-association (4.1 μM, Table 3), indicates that receptor binding also contributes significantly to assembly of TβRI:TβRII complexes. The assembly of TβRI:TβRII complexes with mTGF-β3, and presumably mTGF-β1 as well, therefore appears to be a cooperative process, much like protein folding, in which multiple weaker interactions, including monomer-monomer, non-covalent dimer-receptor, and receptor-receptor interactions, cooperate to enable formation of a thermodynamically stable TGF-β:TβRI:TβRII complex. This manner of cooperative assembly is likely responsible for the ability of mTGF-β1 and mTGF-β3 to induce signaling at concentrations that are more than four orders of magnitude below the K_D for self-association of the monomers (EC_{50}s of about 0.1 nM vs. K_Ds for self-association of 4.1 μM).

The elimination of the heel helix from the TGF-β monomer was shown to be very effective in terms of blocking the cooperative assembly of TβRI:TβRII complexes as shown by the TR-FRET data (Fig. 7*B*) and the cell based signaling data (Fig. 6*A-B*). The AUC data showed that elimination of the heel helix led to the weakening of the monomer-monomer interaction by one order of magnitude (Table 3). The SPR data shown in Figures 6*G-H* further showed that the TβRII-bound form of mmTGF-β2-7M was incapable of binding and recruiting TβRI, which is completely expected based on published structures of TGF-β receptor complexes which show that TβRI binds to a composite interface formed by both chains of TGF-β, as well as TβRII (12,13). Thus, the data show that the reduced propensity of the engineered monomer to self-associate, together with what would be expected to be very weak binding of TβRI to any dimers that do form, is responsible for the inability of mmTGF-β2-7M to assemble a TβRI:TβRII complex. This accounts for the lack of signaling activity, and this together with the retention of high affinity TβRII binding, accounts for the inhibitory activity.

The other type II receptors of the family, ActRII, ActRIIB, BMPRII, and AMHRII, have either been shown or are predicted to bind the GF knuckle, not the GF fingertips as does TβRII (5). They nonetheless share the same property as TβRII in that they bind only by contacting residues from a single GF monomer, not both monomers as has been shown or is predicted for all type I receptors of the family (5). This, together with the structures reported here that show that it is possible to remove α3 without affecting the overall structure of the monomer (Figs. 2*B-D*, 5*B-E*), suggests that it might be possible to generate monomers of other GFs of the family lacking the heel helix that function as inhibitors. These types of inhibitors have numerous potential applications, ranging from research tools for probing roles of specific ligands *in vivo* to clinically useful inhibitors for treating disease which are driven by hyperactive signaling by other ligands of the family, such as cancer cachexia by activin (45).

EXPERIMENTAL PROCEDURES

Protein expression and purification - TGF-β1 was expressed as a secreted protein bound to its prodomain in stably transfected CHO cells. The cell line used to produce TGF-β1, and the accompanying procedure to isolate the mature disulfide-linked TGF-β1 homodimer from the conditioned medium has been previously described (46), and was kindly provided from Dr. Peter Sun (NIAID, Rockville, MD). Mouse homodimeric TGF-β2 (TGF-β2), human homodimeric TGF-β3 (TGF-β3), and variants, including homodimeric N-terminal avi-tagged (47) TGF-β3 (avi-TGF-β3), monomeric TGF-β2 (mTGF-β2), monomeric TGF-β3 (mTGF-β3), mini monomeric TGF-β1 (mmTGF-β1), mini monomeric TGF-β2 (mmTGF-β2), mini monomeric TGF-β3 (mmTGF-β3), mini

monomeric TGF-β2 with seven substitutions to enable high affinity TβRII binding (mmTGF-β2-7M), and mini monomeric N-terminal avi-tagged (47) TGF-β2 with seven substitutions to enable high affinity TβRII binding (avi-mmTGF-β2-7M) were expressed in *E. coli*, refolded from inclusion bodies into native folded disulfide-linked homodimers (TGF-β2, TGF-β3, avi-TGF-β3) or monomers (mTGF-β1, mTGF-β2, mTGF-β3, mmTGF-β1, mmTGF-β2, mmTGF-β3, mmTGF-β2-7M, avi-mmTGF-β2-7M), and purified to homogeneity using high resolution cation exchange chromatography (Source Q, GE Healthcare, Piscataway, NJ) as previously described (39). The nomenclature and features of the dimeric and monomeric TGF-βs used in this study are summarized in the Supplemental Table S1 and the complete sequences are shown in Supplemental Figure S1.

The human TβRI ectodomain (TβRI), spanning residues 1-101 of the mature receptor, or a variant spanning residues 1-88 of the mature receptor with a 15 amino acid avitag (47) appended to the C-terminus (TβRI-ΔC-Avi) was expressed in *E. coli*, refolded from inclusion bodies, and purified to homogeneity as previously described (11). The human TβRII ectodomain (TβRII), spanning residues 15-136 of the mature receptor, or the same but with a C-terminal hexahistidine tag (TβRII-His) was expressed in *E. coli*, refolded from inclusion bodies, and purified to homogeneity as previously described (48).

Solubility Assays - TGF-β dimers and monomers were prepared in 100 mM acetic acid to concentrations of 300 μM or higher and diluted to the desired concentration in either 100 mM acetic acid or phosphate buffered saline (PBS, 10 mM Na_2HPO_4, 1.8 mM KH_2PO_4, 137 mM NaCl, 2.7 mM KCl, pH 7.4). The pH of the samples diluted into PBS were adjusted with small aliquots of NaOH to ensure a final pH of 7.4. The light scattering at 340 nm of the samples were measured in a 1 cm quartz cuvette using a HP 8452 diode array spectrophotometer (HP, Palo Alto, CA). The samples were transferred to a microfuge tube, centrifuged at 20000 x g for 5 minutes and the absorbance at 280 nm of the supernatant was measured using a Nanodrop spectrophotomer (ThermoFisher, Waltham, MA).

NMR Spectroscopy. mmTGF-β2 and mmTGF-β2-7M samples isotopically labeled with ^{15}N or ^{15}N and ^{13}C for NMR were prepared by growing bacterial cells in M9 media containing 0.1 % (w/v) $^{15}NH_4Cl$ or 0.1 % (w/v) $^{15}NH_4Cl$ and 0.03% (w/v) ^{13}C labeled glucose. All NMR samples were prepared in 10 mM sodium phosphate, 10 mM 3-[(3-cholamidopropyl)dimethylammonio]-1-propanesulfonate (CHAPS), and 5% ^2H_2O at a protein concentration of 0.2 mM, pH 4.7. All NMR data was acquired at a sample temperature of 37 °C at either 700 or 800 MHz using Bruker AV-I or AV-II spectrometers equipped with a 5 mm ^1H-{^{13}C,^{15}N} TCI cryogenically cooled probe (Bruker, Billerica, MA). Backbone resonance assignments of mmTGF-β2 and mmTGF-β2-7M were obtained by collecting and analyzing sensitivity-enhanced HNCACB (49), CBCA(CO)NH (50), C(CO)NH (51), HNCO (52), data sets with 25% non-uniform sampling (NUS) of the points in the ^{13}C, ^{15}N acquisition grid. Backbone amide ^{15}N T_2 relaxation parameters were measured in an interleaved manner at 300 °K at a ^{15}N frequency of 70.95 MHz using ^1H-detected pulse schemes previously described (53). The T_2 data sets were each collected using 8 - 10 delay times, varying between 16 -192 ms. The T_2 relaxation times were obtained by fitting relative peak intensities as a function of the T_2 delay time to a two parameter decaying exponential. Data was processed using NMRPipe (54), with the SMILE algorithm used for prediction of the missing points in the ^{13}C and ^{15}N dimensions of the NUS data sets (55). Data analysis was performed using NMRFAM-SPARKY (56).

SPR binding measurements - SPR measurements with TGF-β2 and mmTGF-β2 shown in Fig. 3*A*, *B* were performed using a Biacore 3000 SPR (G.E. Healthcare, Piscataway, NJ) instrument with direct immobilization of TGF-β2 or mmTGF-β2 on the surface of a CM5 sensor chip (G.E. Healthcare, Piscataway, NJ) using an amine (carbodiimide-based) coupling kit (G.E. Healthcare, Piscataway, NJ). SPR experiments shown in Figure 3*C*, *E*, and *G* and Figure 3*D*, *F*, and *H* with TGF-β3 and mmTGF-β2-7M, respectively, were performed using a Biacore X100 SPR instrument (G.E. Healthcare, Piscataway, NJ) with biotinylated ligands captured at a moderate density (50 – 200 RU) onto a streptavidin-coated CM5 sensor chip (GE Healthcare, Piscataway, NJ). Biotinylated TGF-β3 or mmTGF-β2-7M were generated by expressing

TGF-β3 or mmTGF-β2-7M with a N-terminal 15 amino acid avitag (47). TGF-β3-avi or mmTGF-β2-7M-avi was bound to TβRII in 10 mM bicine at pH 8.0 and biotinylated by incubating with a catalytic amount of bacterially expressed BirA recombinase, biotin, and ATP at 37 ° for 2 hr as described (39). Biotinylated avi-tagged TGF-β3 or avi-tagged TGF-β2-7M were bound to a C4 reverse phase column equilibrated with 94.9% water/5% acetonitrile/0.1% triflouroacetic acid and eluted with a linear acetonitrile gradient. SPR measurements shown in Figure 3*A*-*F* were performed in HBS-EP buffer (10 mM Hepes, pH 7.4, 150 mM NaCl, 3 mM EDTA, 0.005% surfactant P20 (GE Healthcare, Piscataway, NJ) with the receptor indicated injected over a series of two-fold dilutions over the concentration range shown. Injections were carried out in duplicates and included 10 buffer blank injections at the start of the experiment. Binding was allowed to associate for 2 - 3 minutes at a flow rate of 100 μL min^{-1}, followed by dissociation for 1 minute or longer. Each cycle of injection was followed by a 30 sec injection of 4 M guanidine•HCl, 2 M NaCl. Data was processed by subtracting both the response from a blank flow cell as well as buffer blanks using the program Scrubber2 (Biologic software, Campbell, Australia). Kinetic fitting of the data was performed with Scrubber2 assuming a simple 1:1 binding model. SPR measurements shown in Figure 3*G*, *H* were performed similarly, except 2 μM TβRII was included in both the running buffer and the injected samples.

Crystallization, structure determination and refinement - Crystals of mmTGF-β2 were formed in sitting drops at 25 °C by combining 0.2 μL of a 7.9 mg mL^{-1} protein stock solution in 10 mM MES pH 5.5 with 0.2 μL of the precipitant from the well, 20 % PEG 3350, 0.2 M sodium thiocyanate. Harvested crystals were mounted in undersized nylon loops with excess mother liquor wicked off, followed by flash-cooling in liquid nitrogen prior to data collection. Data were acquired at the Advanced Photon Source NE-CAT beamline 24-ID-C and integrated and scaled using XDS (57). The structure was determined by the molecular replacement method implemented in PHASER (58) using a truncated version of PDB entry 2TGI (59) as the search model. Coordinates were refined using PHENIX (60), including simulated annealing with torsion angle dynamics, and alternated with manual rebuilding using COOT (61). Data collection and refinement statistics are shown in Table 1.

Crystals of the mmTGF-β2-7M:TβRII complex were formed in hanging drops at 25 °C by combining 1.0 μL of a 7.4 mg mL^{-1} stock solution of the complex in 10 mM Tris, pH 7.4 with 1.0 μL of 0.1 M Hepes, pH 7.5, 60 % v/v (+/-)-2-methyl-2,4-pentanediol. Harvested crystals were mounted in nylon loops, followed by flash-cooling in liquid nitrogen prior to data collection. Data were acquired at the Advanced Photon Source 22-ID-D and integrated and scaled using HKL2000 (62). The structure was determined by the molecular replacement method implemented in PHASER (58) using TβRII (PDB 1M9Z (63)) and mmTGF-β2 as search models. Coordinates were refined using PHENIX (60), alternated with manual rebuilding using COOT (61). Data collection and refinement statistics are shown in Table 1.

Crystals of mmTGF-β2-7M were formed in hanging drops at 25 °C by combining 1.0 μL of a 10 mg mL^{-1} protein stock solution in 20 mM acetic acid with 0.8 μL of the precipitant from the well, 100 mM sodium acetate dibasic trihydrate, pH 4.6, 25% 2-propanol, and 400 mM calcium chloride dehydrate, and 0.2 μL 5% n-ocyl-β-D-glucoside. Harvested crystals were mounted in nylon loops and cryoprotected in well buffer containing 20% glycerol and flash-cooled in a nitrogen stream. Data was collected at 100 K using a Rigaku FR-E Superbright generator equipped with a Saturn 944 CCD detector and processed using MOSFLM (64) in CCP4 (65). The structure of mmTGF-β2-7M was solved via molecular replacement using the structure of mmTGF-β2-7M from its co-crystal structure with TβRII. Iterative model building and refinement were performed using COOT (61) and PHENIX[4], respectively. Data collection and refinement statistics are shown in Table 1.

Luciferase assays - HEK293 cells stably transfected with the $CAGA_{12}$ TGF-β reporter were used for the luciferase reporter assays (44) and were maintained in Dulbecco's modified eagles medium (DMEM) containing 10% fetal bovine serum (FBS) and 1% penicillin/streptomycin. Cells were treated for 16 hours with a TGF-β (TGF-β1, mTGF-β3, or mmTGF-β2-7M) concentrations series or a mmTGF-β2-7M concentration series in the presence of a constant sub-saturating concentration of TGF-β (TGF-β1 –

8 pM, TGF-β2 – 20 pM, or TGF-β3 – 10 pM). Proteins were diluted in Dulbecco's Modified Eagle's medium (DMEM) containing 0.1% w/v BSA. After 16 hours cells were lysed with Tropix lysis buffer (ThermoFisher, Waltham, MA) and luciferase activity was read with a Promega GloMax luminometer (Promega, Madison, WI). Luciferase activity was normalized to total protein levels determined by bicinchoninic acid (BCA) protein assay. Graphpad Prism 6 was used to fit the data to standard models for ligand activity (EC_{50}) and ligand inhibitory activity (IC_{50}) (Graphpad, LaJolla, CA).

Time-resolved FRET assays - The following purified proteins were used to address the ligand requirements for the formation of complexes containing TβRI and TβRII: TGF-β3, mTGF-β3, mmTGF-β2-7M, biotinylated TβRI-ΔC-Avi and TβRII-His. Initially 20 μM binary complexes of TGF-β3:TβRII-His, mTGF-β3:TβRII-His, and mmTGF-β2-7M:TβRII-His were formed in a 50 mM Tris, pH 7.5 buffer and stored at 4° C. A time-resolved fluorescence resonance energy transfer (TR-FRET) assay based on the proximity-dependent transfer of fluorescence from the donor terbium cryptate labeled anti-His mAb (Tb-anti-His, CisBio, Bedford, MA) to the acceptor XL665 labeled streptavidin (SA-665, CisBio, Bedford, MA) was used to monitor the assembly of ternary ligand:TβRII-His:biotinylated TβRI-ΔC-Avi complexes. 50 μL assays containing 100 nM or 250 nM TGF-β3:TβRII-His (1:2), mTGF-β3:TβRII-His (1:1), and mmTGF-β2-7M:TβRII-His (1:1) complexes were incubated with 50 nM biotinylated TβRI-ΔC-Avi. Each 50ul ternary complex formation assay also contained 2 nM Tb-anti-His and 30nM SA-665 and was incubated at room temperature for 2 h. Each condition was tested in replicates of six. Buffer control (n=6) contained only 2 nM Tb-anti-His and 30 nM SA-XL665. The buffer conditions for each assay were 50 mM Tris, 50 mM NaCl, pH 7.5. The assays were performed in Corning black 384 well low flange microplates (ThermoFisher, Waltham, MA). After a 2 h incubation, the assay plate was measured for terbium/XL-665 TR-FRET on a BMG Labtech Pherastar FS multimode plate reader (BMG Labtech Inc., Cary, NC). An optic module containing 337, 490 and 665 nm filters was used to monitor TR-FRET producing raw data for 337/490 (terbium emission) and 337/665 (XL-665) emission. The ratio of 665 emission/490 emission was determined for each condition and was subsequently used to calculate ΔF, which is a measure that reflects the signal of the sample versus the background. ΔF was calculated using the following equation: $(Ratio_{signal}-Ratio_{negative}/Ratio_{negative}) \times 100$. The $Ratio_{signal}$ refers to the assays containing the trimeric complexes or buffer control. The $Ratio_{negative}$ refers to two buffer control assays (2 nM Tb-anti-His and 30 nM SA-665). For the buffer control, 2 out of the 6 replicates were assigned as negative controls for the purpose of calculating ΔF. ΔF was calculated for the remaining 4 buffer control replicates.

Analytical ultracentrifugation - mTGF-β3, mmTGF-β2, and mmTGF-β2-7M were analyzed by sedimentation velocity to establish equilibrium constants for self-association of monomeric TGF-βs to form homodimers. mTGF-β3, mmTGF-β2, and mmTGF-β2-7M were each measured at 280 nm in an epon two channel centerpiece fitted with quartz windows, and centrifuged at 20°C and 42,000 rpm for 27 hours in a 15 mM sodium phosphate buffer adjusted to pH 3.8, containing 100 mM NaCl. 300 scans were collected in intensity mode on a Beckman Optima XL-I analytical ultracentrifuge at the CAUMA facility at the UTHSCSA. Data analysis was performed with UltraScan release 2142 (66,67), calculations were performed at the San Diego Supercomputing Center on Comet and Gordon. The sedimentation velocity data were initially fitted with the two-dimensional spectrum analysis as described in (66) to remove time- and radially invariant noise from the raw data, and to fit the meniscus position. Subsequently, the data were fitted to a discrete monomer-dimer model using the adaptive space-time finite element method (67) and genetic algorithms for the parameter optimization (68). The monomer-dimer model accounts for mass action and the reversible association behavior, fitting the thermodynamic and hydrodynamic parameters, as well as the partial specific volume while assuming the predicted molar mass for either wildtype or mutant. A Monte Carlo analysis (69) with 100 iterations was performed for each dataset to obtain fitting statistics. Buffer density and viscosity were estimated with UltraScan based on buffer composition and all hydrodynamic values were corrected for standard conditions

(20°C and water). The fitting results provided an excellent fit with random residuals and very low RMSD values (see Supplementary Material, Figs. 4, 5, and 6). All results are summarized in Table 3.

ACKNOWLEDGEMENTS: The authors would like to thank Dr. Peter Sun NIH NIAID, for providing the stably transected CHO cell line overexpressing TGF-β1, Dr. William Furey for guidance on the refinement of the mmTGF-β2-7M and mmTGF-β2-7M:TβRII structures, Doowon Lee for assistance with the X-ray instrumentation, Mike Delk for assistance with the NMR instrumentation, and Liping Wang for technical assistance with the analytical ultracentrifugation measurements. The assigned chemical shifts for mmTGF-β2 and mmTGF-β2-7M were deposited to BioMagResBank (BMRB) under accession codes 26943 and 26944, respectively. The structures of mmTGF-β2, mmTGF-β2-7M, and the mmTGF-β2-7M:TβRII complex were submitted to the RCSB Protein Data Bank (PDB) under accession codes 5TX2, 5TX6, and 5TX4 respectively.

CONFLICT OF INTEREST: The content is solely the responsibility of the authors and does not necessarily represent the official views of the National Institutes of Health. A.P.H. and T.S. are co-inventors of a provisional patent (application US 62/423,920) that covers the dominant negative TGF-β, mmTGF-β2-7M.

AUTHOR CONTRIBUTIONS: SKK crystallized mmTGF-β2 and the mmTGF-β2-7M:TβRII complex, performed the solubility measurements, performed a portion of the SPR experiments, and wrote the initial draft of the paper. LB and CSH performed the luciferase assays. CSH together with MB, MV, BL, BR, and KEC established the expression and purification of mmTGF-β2-7M. AT, BI, and KEC performed the NMR assignment of mmTGF-β2. EMP crystallized and determined the structure of mmTGF-β2-7M. ABT and PJH determined the structure of mmTGF-β2. RK performed some of the SPR experiments. SD, COB, and GC determined the structure of mmTGF-β2-7M:TβRII. MJH performed the TR-FRET experiments and BD performed the AUC experiments. APH conceived the design of the dominant negative TGF-β inhibitors, in consultation with TS. APH also performed the NMR assignment of mmTGF-β2-7M and wrote the final draft of the paper. All authors reviewed the results and approved the final version of the manuscript.

REFERENCES

1. Biernacka, A., Dobaczewski, M., and Frangogiannis, N. G. (2011) TGF-beta signaling in fibrosis. Growth Factors 29, 196-202
2. Dietz, H. C., Cutting, G. R., Pyeritz, R. E., Maslen, C. L., Sakai, L. Y., Corson, G. M., Puffenberger, E. G., Hamosh, A., Nanthakumar, E. J., Curristin, S. M., and et al. (1991) Marfan syndrome caused by a recurrent de novo missense mutation in the fibrillin gene. Nature 352, 337-339
3. Loeys, B. L., Mortier, G., and Dietz, H. C. (2013) Bone lessons from Marfan syndrome and related disorders: fibrillin, TGF-B and BMP at the balance of too long and too short. Pediatr Endocrinol Rev 10 Suppl 2, 417-423
4. Massague, J. (2008) TGFbeta in Cancer. Cell 134, 215-230
5. Hinck, A. P., Mueller, T. D., and Springer, T. A. (2016) Structural Biology and Evolution of the TGF-beta Family. Cold Spring Harb Perspect Biol
6. Massague, J. (1998) TGF-beta signal transduction. Annu Rev Biochem 67, 753-791
7. Robertson, I. B., and Rifkin, D. B. (2013) Unchaining the beast; insights from structural and evolutionary studies on TGFbeta secretion, sequestration, and activation. Cytokine Growth Factor Rev 24, 355-372
8. Wrana, J. L., Attisano, L., Carcamo, J., Zentella, A., Doody, J., Laiho, M., Wang, X. F., and Massague, J. (1992) TGF beta signals through a heteromeric protein kinase receptor complex. Cell 71, 1003-1014

9. Wrana, J. L., Attisano, L., Wieser, R., Ventura, F., and Massague, J. (1994) Mechanism of activation of the TGF-beta receptor. Nature 370, 341-347
10. Laiho, M., Weis, F. M., Boyd, F. T., Ignotz, R. A., and Massague, J. (1991) Responsiveness to transforming growth factor-beta (TGF-beta) restored by genetic complementation between cells defective in TGF-beta receptors I and II. J Biol Chem 266, 9108-9112
11. Zuniga, J. E., Groppe, J. C., Cui, Y., Hinck, C. S., Contreras-Shannon, V., Pakhomova, O. N., Yang, J., Tang, Y., Mendoza, V., Lopez-Casillas, F., Sun, L., and Hinck, A. P. (2005) Assembly of TbetaRI:TbetaRII:TGFbeta ternary complex in vitro with receptor extracellular domains is cooperative and isoform-dependent. J Mol Biol 354, 1052-1068
12. Groppe, J., Hinck, C. S., Samavarchi-Tehrani, P., Zubieta, C., Schuermann, J. P., Taylor, A. B., Schwarz, P. M., Wrana, J. L., and Hinck, A. P. (2008) Cooperative assembly of TGF-beta superfamily signaling complexes is mediated by two disparate mechanisms and distinct modes of receptor binding. Mol Cell 29, 157-168
13. Radaev, S., Zou, Z., Huang, T., Lafer, E. M., Hinck, A. P., and Sun, P. D. (2010) Ternary complex of transforming growth factor-beta1 reveals isoform-specific ligand recognition and receptor recruitment in the superfamily. J Biol Chem 285, 14806-14814
14. Loeys, B. L., Schwarze, U., Holm, T., Callewaert, B. L., Thomas, G. H., Pannu, H., De Backer, J. F., Oswald, G. L., Symoens, S., Manouvrier, S., Roberts, A. E., Faravelli, F., Greco, M. A., Pyeritz, R. E., Milewicz, D. M., Coucke, P. J., Cameron, D. E., Braverman, A. C., Byers, P. H., De Paepe, A. M., and Dietz, H. C. (2006) Aneurysm syndromes caused by mutations in the TGF-beta receptor. N Engl J Med 355, 788-798
15. Markowitz, S. D., and Roberts, A. B. (1996) Tumor suppressor activity of the TGF-beta pathway in human cancers. Cytokine & growth factor reviews 7, 93-102
16. Bandyopadhyay, A., Agyin, J. K., Wang, L., Tang, Y., Lei, X., Story, B. M., Cornell, J. E., Pollock, B. H., Mundy, G. R., and Sun, L. Z. (2006) Inhibition of pulmonary and skeletal metastasis by a transforming growth factor-beta type I receptor kinase inhibitor. Cancer Res 66, 6714-6721
17. Ganapathy, V., Ge, R., Grazioli, A., Xie, W., Banach-Petrosky, W., Kang, Y., Lonning, S., McPherson, J., Yingling, J. M., Biswas, S., Mundy, G. R., and Reiss, M. (2010) Targeting the Transforming Growth Factor-beta pathway inhibits human basal-like breast cancer metastasis. Mol Cancer 9, 122
18. Muraoka, R. S., Dumont, N., Ritter, C. A., Dugger, T. C., Brantley, D. M., Chen, J., Easterly, E., Roebuck, L. R., Ryan, S., Gotwals, P. J., Koteliansky, V., and Arteaga, C. L. (2002) Blockade of TGF-beta inhibits mammary tumor cell viability, migration, and metastases. J Clin Invest 109, 1551-1559
19. Nam, J. S., Terabe, M., Mamura, M., Kang, M. J., Chae, H., Stuelten, C., Kohn, E., Tang, B., Sabzevari, H., Anver, M. R., Lawrence, S., Danielpour, D., Lonning, S., Berzofsky, J. A., and Wakefield, L. M. (2008) An anti-transforming growth factor beta antibody suppresses metastasis via cooperative effects on multiple cell compartments. Cancer Res 68, 3835-3843
20. Yang, Y. A., Dukhanina, O., Tang, B., Mamura, M., Letterio, J. J., MacGregor, J., Patel, S. C., Khozin, S., Liu, Z. Y., Green, J., Anver, M. R., Merlino, G., and Wakefield, L. M. (2002) Lifetime exposure to a soluble TGF-beta antagonist protects mice against metastasis without adverse side effects. J Clin Invest 109, 1607-1615
21. Miao, Z. F., Zhao, T. T., Wang, Z. N., Miao, F., Xu, Y. Y., Mao, X. Y., Gao, J., Wu, J. H., Liu, X. Y., You, Y., Xu, H., and Xu, H. M. (2014) Transforming growth factor-beta1 signaling blockade attenuates gastric cancer cell-induced peritoneal mesothelial cell fibrosis and alleviates peritoneal dissemination both in vitro and in vivo. Tumour Biol 35, 3575-3583
22. Di Sabatino, A., Jackson, C. L., Pickard, K. M., Buckley, M., Rovedatti, L., Leakey, N. A., Picariello, L., Cazzola, P., Monteleone, G., Tonelli, F., Corazza, G. R., MacDonald, T. T., and Pender, S. L. (2009) Transforming growth factor beta signalling and matrix metalloproteinases in the mucosa overlying Crohn's disease strictures. Gut 58, 777-789

23. Yamada, M., Kuwano, K., Maeyama, T., Yoshimi, M., Hamada, N., Fukumoto, J., Egashira, K., Hiasa, K., Takayama, K., and Nakanishi, Y. (2007) Gene transfer of soluble transforming growth factor type II receptor by in vivo electroporation attenuates lung injury and fibrosis. J Clin Pathol 60, 916-920
24. Connolly, E. C., Freimuth, J., and Akhurst, R. J. (2012) Complexities of TGF-beta targeted cancer therapy. Int J Biol Sci 8, 964-978
25. Hawinkels, L. J., and Ten Dijke, P. (2011) Exploring anti-TGF-beta therapies in cancer and fibrosis. Growth Factors 29, 140-152
26. Ge, R., Rajeev, V., Subramanian, G., Reiss, K. A., Liu, D., Higgins, L., Joly, A., Dugar, S., Chakravarty, J., Henson, M., McEnroe, G., Schreiner, G., and Reiss, M. (2004) Selective inhibitors of type I receptor kinase block cellular transforming growth factor-beta signaling. Biochem Pharmacol 68, 41-50
27. Singh, J., Ling, L. E., Sawyer, J. S., Lee, W. C., Zhang, F., and Yingling, J. M. (2004) Transforming the TGFbeta pathway: convergence of distinct lead generation strategies on a novel kinase pharmacophore for TbetaRI (ALK5). Curr Opin Drug Discov Devel 7, 437-445
28. Yingling, J. M., Blanchard, K. L., and Sawyer, J. S. (2004) Development of TGF-beta signalling inhibitors for cancer therapy. Nat Rev Drug Discov 3, 1011-1022
29. Connolly, E. C., Saunier, E. F., Quigley, D., Luu, M. T., De Sapio, A., Hann, B., Yingling, J. M., and Akhurst, R. J. (2011) Outgrowth of drug-resistant carcinomas expressing markers of tumor aggression after long-term TbetaRI/II kinase inhibition with LY2109761. Cancer research 71, 2339-2349
30. Lonning, S., Mannick, J., and McPherson, J. M. (2011) Antibody targeting of TGF-beta in cancer patients. Curr Pharm Biotechnol 12, 2176-2189
31. Hinck, A. P. (2012) Structural studies of the TGF-betas and their receptors - insights into evolution of the TGF-beta superfamily. FEBS Lett 586, 1860-1870
32. Meibohm, B. (2012) Pharmacokinetics and Half-Life of Protein Therapeutics. in Therapeutic Proteins: Strategies to Modulate Their Plasma Half-Lives (Kontermann, R. ed.), Wiley-Blackwell, Weinheim, Germany. pp 23-38
33. Meibohm, B., and Braeckman, R. A. (2007) Pharmacokinetics and Pharmacodynamics of Peptides and Proteins. in Pharmaceutical Biotechnology: Concepts and Applications (Crommelin, D. J. A., Sindelar, R. D., and Meibohm, B. eds.). pp 95-123
34. Papo, N., Silverman, A. P., Lahti, J. L., and Cochran, J. R. (2011) Antagonistic VEGF variants engineered to simultaneously bind to and inhibit VEGFR2 and alphavbeta3 integrin. Proc Natl Acad Sci U S A 108, 14067-14072
35. Amatayakul-Chantler, S., Qian, S. W., Gakenheimer, K., Bottinger, E. P., Roberts, A. B., and Sporn, M. B. (1994) [Ser77]transforming growth factor-beta 1. Selective biological activity and receptor binding in mink lung epithelial cells. J Biol Chem 269, 27687-27691
36. Hinck, A. P., Archer, S. J., Qian, S. W., Roberts, A. B., Sporn, M. B., Weatherbee, J. A., Tsang, M. L., Lucas, R., Zhang, B. L., Wenker, J., and Torchia, D. A. (1996) Transforming growth factor beta 1: three-dimensional structure in solution and comparison with the X-ray structure of transforming growth factor beta 2. Biochemistry 35, 8517-8534
37. Mittl, P. R., Priestle, J. P., Cox, D. A., McMaster, G., Cerletti, N., and Grutter, M. G. (1996) The crystal structure of TGF-beta 3 and comparison to TGF-beta 2: implications for receptor binding. Protein Sci 5, 1261-1271
38. Huang, T., David, L., Mendoza, V., Yang, Y., Villarreal, M., De, K., Sun, L., Fang, X., Lopez-Casillas, F., Wrana, J. L., and Hinck, A. P. (2011) TGF-beta signalling is mediated by two autonomously functioning TbetaRI:TbetaRII pairs. EMBO J 30, 1263-1276
39. Huang, T., and Hinck, A. P. (2016) Production, Isolation, and Structural Analysis of Ligands and Receptors of the TGF-beta Superfamily. Methods Mol Biol 1344, 63-92
40. Baardsnes, J., Hinck, C. S., Hinck, A. P., and O'Connor-McCourt, M. D. (2009) TbetaR-II discriminates the high- and low-affinity TGF-beta isoforms via two hydrogen-bonded ion pairs. Biochemistry 48, 2146-2155

41. De Crescenzo, G., Hinck, C. S., Shu, Z., Zuniga, J., Yang, J., Tang, Y., Baardsnes, J., Mendoza, V., Sun, L., Lopez-Casillas, F., O'Connor-McCourt, M., and Hinck, A. P. (2006) Three key residues underlie the differential affinity of the TGFbeta isoforms for the TGFbeta type II receptor. J Mol Biol 355, 47-62
42. Pellaud, J., Schote, U., Arvinte, T., and Seelig, J. (1999) Conformation and self-association of human recombinant transforming growth factor-beta3 in aqueous solutions. J Biol Chem 274, 7699-7704
43. Hart, P. J., Deep, S., Taylor, A. B., Shu, Z., Hinck, C. S., and Hinck, A. P. (2002) Crystal structure of the human TbetaR2 ectodomain--TGF-beta3 complex. Nat Struct Biol 9, 203-208
44. Thies, R. S., Chen, T., Davies, M. V., Tomkinson, K. N., Pearson, A. A., Shakey, Q. A., and Wolfman, N. M. (2001) GDF-8 propeptide binds to GDF-8 and antagonizes biological activity by inhibiting GDF-8 receptor binding. Growth Factors 18, 251-259
45. Coerver, K. A., Woodruff, T. K., Finegold, M. J., Mather, J., Bradley, A., and Matzuk, M. M. (1996) Activin signaling through activin receptor type II causes the cachexia-like symptoms in inhibin-deficient mice. Mol Endocrinol 10, 534-543
46. Zou, Z., and Sun, P. D. (2004) Overexpression of human transforming growth factor-beta1 using a recombinant CHO cell expression system. Protein Expr Purif 37, 265-272
47. Cull, M. G., and Schatz, P. J. (2000) Biotinylation of proteins in vivo and in vitro using small peptide tags. Methods Enzymol 326, 430-440
48. Hinck, A. P., Walker, K. P., 3rd, Martin, N. R., Deep, S., Hinck, C. S., and Freedberg, D. I. (2000) Sequential resonance assignments of the extracellular ligand binding domain of the human TGF-beta type II receptor. J Biomol NMR 18, 369-370
49. Wittekind, M., and Mueller, L. (1993) HNCACB, a high-sensitivity 3-D NMR experiment to correlate amide-proton and nitrogen resonances with the alpha-carbon and beta-carbon resonances in proteins. J. Magn. Reson. Ser. B 101
50. Grzesiek, S., and Bax, A. (1993) Amino acid type determination in the sequential assignment procedure of uniformly 13C/15N-enriched proteins. J Biomol NMR 3, 185-204
51. Grzesiek, S., Anglister, J., and Bax, A. (1993) Correlation of backbone amide and aliphatic side-chain resonances in C-13/N-15-enriched proteins by isotropic mixing of C-13 magnetization. J. Magn. Reson. Ser. B 101, 114--119
52. Kay, L. E., Ikura, M., Tschudin, R., and Bax, A. (1990) 3-Dimensional Triple-Resonance Nmr-Spectroscopy of Isotopically Enriched Proteins. J Magn Reson 89, 496-514
53. Kay, L. E., Torchia, D. A., and Bax, A. (1989) Backbone dynamics of proteins as studied by 15N inverse detected heteronuclear NMR spectroscopy: application to staphylococcal nuclease. Biochemistry 28, 8972-8979
54. Delaglio, F., Grzesiek, S., Vuister, G. W., Zhu, G., Pfeifer, J., and Bax, A. (1995) NMRPipe: a multidimensional spectral processing system based on UNIX pipes. J Biomol NMR 6, 277-293
55. Ying, J., Delaglio, F., Torchia, D. A., and Bax, A. (2016) Sparse Multidimensional Iterative Lineshape-Enhanced (SMILE) Reconstruction of Both Non-Uniformly Sampled and Conventional NMR Data. J. Biomol. NMR in press
56. Lee, W., Tonelli, M., and Markley, J. L. (2015) NMRFAM-SPARKY: enhanced software for biomolecular NMR spectroscopy. Bioinformatics 31, 1325-1327
57. Kabsch, W. (2010) Xds. Acta Crystallogr D Biol Crystallogr 66, 125-132
58. McCoy, A. J., Grosse-Kunstleve, R. W., Adams, P. D., Winn, M. D., Storoni, L. C., and Read, R. J. (2007) Phaser crystallographic software. J Appl Crystallogr 40, 658-674
59. Daopin, S., Piez, K. A., Ogawa, Y., and Davies, D. R. (1992) Crystal structure of transforming growth factor-beta 2: an unusual fold for the superfamily. Science 257, 369-373
60. Adams, P. D., Afonine, P. V., Bunkoczi, G., Chen, V. B., Davis, I. W., Echols, N., Headd, J. J., Hung, L. W., Kapral, G. J., Grosse-Kunstleve, R. W., McCoy, A. J., Moriarty, N. W., Oeffner, R., Read, R. J., Richardson, D. C., Richardson, J. S., Terwilliger, T. C., and Zwart, P. H. (2010) PHENIX: a comprehensive Python-based system for macromolecular structure solution. Acta Crystallogr D Biol Crystallogr 66, 213-221

61. Emsley, P., Lohkamp, B., Scott, W. G., and Cowtan, K. (2010) Features and development of Coot. Acta Crystallogr D Biol Crystallogr 66, 486-501
62. Otwinowski, Z., and Minor, W. (1997) Processing of X-ray diffraction data collected in oscillation mode. Method Enzymol 276, 307-326
63. Boesen, C. C., Radaev, S., Motyka, S. A., Patamawenu, A., and Sun, P. D. (2002) The 1.1 angstrom crystal structure of human TGF-beta type II receptor ligand binding domain. Structure 10, 913-919
64. Battye, T. G. G., Kontogiannis, L., Johnson, O., Powell, H. R., and Leslie, A. G. W. (2011) iMOSFLM: a new graphical interface for diffraction-image processing with MOSFLM. Acta Crystallogr D 67, 271-281
65. Winn, M. D., Ballard, C. C., Cowtan, K. D., Dodson, E. J., Emsley, P., Evans, P. R., Keegan, R. M., Krissinel, E. B., Leslie, A. G. W., McCoy, A., McNicholas, S. J., Murshudov, G. N., Pannu, N. S., Potterton, E. A., Powell, H. R., Read, R. J., Vagin, A., and Wilson, K. S. (2011) Overview of the CCP4 suite and current developments. Acta Crystallogr D 67, 235-242
66. Demeler, B. (2010) Methods for the design and analysis of sedimentation velocity and sedimentation equilibrium experiments with proteins. Curr Protoc Protein Sci Chapter 7, Unit 7 13
67. Cao, W., and Demeler, B. (2008) Modeling analytical ultracentrifugation experiments with an adaptive space-time finite element solution for multicomponent reacting systems. Biophys J 95, 54-65
68. Demeler, B., Brookes, E., Wang, R., Schirf, V., and Kim, C. A. (2010) Characterization of reversible associations by sedimentation velocity with UltraScan. Macromol Biosci 10, 775-782
69. Demeler, B., and Brookes, E. (2008) Monte Carlo analysis of sedimentation experiments. Colloid Polym Sci 286, 129-137

FOOTNOTES

This research was supported by the NIH (GM58670 and CA172886 to A.H.) and the Robert A. Welch Foundation (AQ1842 to A.H.). S.K.K. was supported by training grants provided by CPRIT (RP1450105) and the AHA (15PRE25550015). Additional support was provided by UT Health Science Center CTRC Macromolecular Structure and Interactions Core supported by NCI P30 CA54174, the UTHSCSA Center for Macromolecular Interactions Core Facility supported by the UT Health Science Center UCRF, and UTHSCSA/UTSA Center for Innovative Drug Discovery and High Throughput Screening Facility supported by NIH NCATS UL1 TR001120 (M.J.H). UltraScan software development is supported by grants from the NIH (GM120600, B.D.) and NSF (ACI-1339649, B.D.) and the calculations at SDSC were supported by an XSEDE community allocation grant (MCB070039, B.D.).

The abbreviations used are: GF, growth factor; TGF-β, tranforming growth factor-beta; TβRII, TGF-β type II receptor; TβRI, TGF-β type I receptor; MAP kinase, mitogen-activated protein kinase; JNK, Jun N-terminal kinase; Alk, activin-like kinase; PEG, polyethylene glycol; VEGF, vascular-endothelial growth factor; SPR, surface plasmon resonance; HBS, hepes buffered saline with surfactant P20; RU, resonance units; CHAPS, 3-[(3-Cholamidopropyl)dimethylammonio]-1-propanesulfonate; NMR, nuclear magnetic resonance; HSQC, heteronuclear single quantum shift correlation; RMSD, root mean square deviation; TR-FRET, time-resolved fluorescence resonance energy transfer; AUC, analytical ultracentrifugation; ActRII, activin type II receptor; ActRIIB, activin type IIB receptor; BMPRII, BMP type II receptor, AMHRII, antimüllerian hormone type II receptor, BMP, bone morphogenetic protein; GDF, growth and differentiation factor,

Table 1. X-ray Data collection and refinement statistics.

Data collection			
Molecule	mmTGF-β2	mmTGF-β2-7M	mmTGF-β2-7M:TβRII
X-ray Source	Adv. Photon Source 24-ID-C	Rigaku 007 generator and Saturn 944 CCD detector	Adv. Photon Source SER-CAT 22-ID-D
Space group	*C*2	$P3_121$	$P2_12_12_1$
Cell dimensions			
a, *b*, *c* (Å)	99.5, 33.4, 54.1	81.74, 81.74, 80.93	39.0, 70.8, 77.1
α, β, γ (°)	90, 109.6, 90	90, 90, 120	90, 90, 90
Wavelength (Å)	0.9795	1.542	0.97949
Resolution (Å)	51.01-1.82 (1.92-1.82)*	36.48 - 2.75 (2.89 - 2.75)*	35.39-1.88 (1.97 – 1.88)*
R_{sym}	0.050 (0.443)	0.132 (0.463)	0.143 (0.97)
R_{pim}	0.038 (0.307)	0.055 (0.232)	0.058 (0.522)
$I/\sigma I$	12.7 (2.2)	16.4 (4.0)	15.17 (2.02)
Completeness (%)	98.4 (98.4)	99.9 (99.8)	99.6 (99.4)
Redundancy	3.6 (3.5)	12.3 (8.9)	6.8 (6.6)
Wilson value (Å^2)	28.9	30.23	30.08
Refinement			
Resolution (Å)	51.01-1.82	36.48 - 2.75	35.39-1.88
No. reflections	15,027	8493	17,715
R_{work}/ R_{free}	0.209/0.252	0.2127/0.2716	0.1955/0.2216
No. atoms			
Protein	1,462	2,086	1,570
Water	107	63	82
B-factors (Å^2)			
Protein	33.3	40.2	43.6
Water	36.4	22.2	41.22
R.m.s deviations			
Bond lengths (Å)	0.012	0.003	0.011
Bond angles (°)	1.030	0.763	1.143
Ramachandran statistics - favored, allowed, outliers (%)	94.4, 5.0, 0.6	93.2, 6.8, 0.0	96.39, 3.09, 0.52

*Highest resolution shell is shown in parentheses.

Table 2. SPR binding parameters for TβRII and TβRI binding to TGF-β3 and mmTGF-β2-7M

Immobilized Ligand	Injected Receptor	Buffer	k_a (M^{-1} s^{-1})*	k_d (s^{-1})*	K_D (μM)*	R_{max} (RU)*
avi-mmTGF-β2-7M	TβRII	HBS-EP	1.16×10^5 (1.48×10^3)	5.46×10^{-2} (3.78×10^{-4})	0.47 (0.07)	256 (2)
avi-TGF-β3	TβRII	HBS-EP	2.64×10^5 (3.97×10^3)	1.132×10^{-1} (6.94×10^{-4})	0.43 (0.05)	128 (1)
avi-TGF-β3	TβRI	HBS-EP + 2 μM TβRII	4.64×10^4 (1.27×10^3)	2.05×10^{-2} (3.42×10^{-4})	0.44 (0.11)	44 (2)
avi-mmTGF-β2-7M	TβRI	HBS-EP + 2 μM TβRII	n.d.**	n.d.**	n.d.**	n.d.**

*Error estimates shown in parentheses
**n.d. – no detectable response

Table 3. Fitting results for the finite element monomer-dimer model for TGF-β monomers

Parameter	mTGF-β3	mmTGF-β2	mmTGF-β2-7M
RMSD of the fit (OD_{280} nm)	0.00253	0.00276	0.00361
K_{D1-2} (M)	$4.1x10^{-6}$ (1.9×10^{-6}, 6.2×10^{-6})	4.4×10^{-5} (3.9×10^{-5}, 4.8×10^{-5})	4.9×10^{-5} (4.5×10^{-5}, 5.3×10^{-5})
Loading concentration (M)	1.25×10^{-5}	1.58×10^{-5}	1.57×10^{-5}
Frictional ratio, monomer	1.04 (0.99, 1.09)	1.18 (1.16, 1.19)	1.30 (1.29, 1.31)
Frictional ratio, dimer	1.37 (1.29, 1.44)	1.30 (1.29, 1.31)	1.44 (1.43, 1.45)
Partial specific volume, monomer, dimer ($\bar{v}$, mL g^{-1})	8.10×10^{-1} (7.99×10^{-1}, 8.21×10^{-1})	7.70×10^{-1} (7.67×10^{-1}, 7.72×10^{-1})	7.07×10^{-1} (7.05×10^{-1}, 7.10×10^{-1})
Sedimentation coefficient, monomer (s, x 10^{-13})	1.29 (1.26, 1.32)	1.24 (1.23, 1.25)	1.46 (1.45, 1.46)
Sedimentation coefficient, dimer (s, x 10^{-13})	1.56 (1.54, 1.58)	1.78 (1.75, 1.81)	2.08 (2.07, 2.10)

*Parameters in parenthesis denote the 95% confidence interval obtained from Monte Carlo analysis

FIGURES AND FIGURE LEGENDS

Figure 1. Structure of the TGF-β signaling complex and sequences of the engineered TGF-β variants lacking the heel helix, α3. *A*. Cartoon representation of the TGF-β signaling complex formed between human TGF-β3 homodimer (magenta and blue ribbons) and the extracellular ligand binding domains of the human TGF-β type I and type II receptors, TβRI (red ribbon) and TβRII (tan ribbon) (PDB 2PJY) (12). The disulfide bonds, including the single inter-chain disulfide connecting the TGF-β monomers, are depicted in yellow. The TGF-β monomers are described as curled left hands, with the heel formed by a 3-1/2 turn α-helix (α3) and the four fingers formed by the β-strands that extend from the cystine knot that stabilizes each monomer. *B*. Expanded view illustrating packing interactions formed by hydrophobic residues that emanate from the heel α-helix (blue ribbon) of one TGF-β3 monomer with hydrophobic residues from the palm region of the opposing TGF-β3 monomer (magenta ribbon with transparent magenta surface). *C*. Expanded view illustrating ionic, hydrogen bonding, and hydrophobic interactions that stabilize TβRI (red ribbon) at the composite interface formed by both monomers of TGF-β3 (magneta and blue ribbons) and TβRII (tan ribbon). *D*. Sequence alignment of TGF-β1, -β2, and –β3 with monomeric variants in which Cys77, which normally forms the inter-chain disulfide bond, is substituted with serine (mTGF-β2 and mTGF-β3) or mini monomeric variants in which Cys77 is substituted with serine, residues 52-71 have been deleted, and 2 or 3 additional residues (highlighted in red) have been substituted (mmTGF-β1, mmTGF-β2, and mmTGF-β3). Calculated net charge of the corresponding monomers at pH 7.0 is shown on the right. *E*. Sequence alignment of TGF-β1, -β3, -β2, mmTGF-β2, and mmTGF-β2-7M in the TβRII binding region. Residues in the TβRII binding interface are indicated by yellow shading. Residues substituted in mmTGF-β2-7M relative to mmTGF-β2 are highlighted in red, and include K25R, I92V, and N94R, which were shown previously to be necessary and sufficient for high affinity TβRII binding (40,41). *F*. Interface between TGF-β3 and TβRII, with R25, V92, and R94 highlighted by red labels.

Figure 2. Structure of mmTGF-β2. *A*. Assigned ^{1}H-^{15}N HSQC spectrum of mmTGF-β2 recorded in 10 mM sodium phosphate, 10 mM CHAPS, 5% $^{2}H_2O$, pH 4.7, 37 °C, 800 MHz. Assigned backbone amide signals are indicated by their residue number and one letter amino acid code. *B*. Overlay of 1.8 Å crystal structure of mmTGF-β2 (orange ribbon) with one of the monomers from the 1.8 Å crystal structure of TGF-β2 (PDB 2TGI, blue ribbon). Major structural features are indicated, along with the newly created loop in mmTGF-β2 (red) which takes the place of the heel (α3) helix in TGF-β2. *C*. Overlay of the two mmTGF-β2 chains (Chain A and B shown in orange and green ribbon, respectively) from the crystallographic asymmetric unit. Other details as in panel *B*. *D*. Overlay of mmTGF-β2 and TGF-β2 as in panel B, but with the aligned positions restricted to the residues 18 – 45 and 61 - 87 in fingers 1/2 and 3/4, respectively.

Figure 3. Binding properties of mmTGF-β2 and mmTGF-β2-7M. *A, B*. SPR sensorgrams for injection of a two-fold dilution series from 3 – 0.047 μM of TβRII over immobilized TGF-β2 (*A*) or mmTGF-β2 (*B*). Responses shown were normalized for the surface density of the immobilized TGF-βs. *C-H*. SPR sensorgrams for injection of a two-fold dilution series from 3 – 0.012 μM of TβRII (*C, D*), 1.024 -0.008 μM of TβRI (*E, F*), or 1.024 -0.008 μM TβRI in the presence of 2 μM TβRII in both the running buffer and injected samples (*G, H*) over immobilized avi-TGF-β3 (*C, E, G*) or avi-mmTGF-β2-7M (*D, F, H*). Sensorgrams shown in panels *C*, *D*, and *G* were fitted to a 1:1 binding model – raw data is shown in black and the fitted curve is shown in red. TGF-β2 and mmTGF-β2 were immobilized by direct carboiimide-based amine coupling to the sensor surface, while avi-TGF-β3 or avi-mmTGF-β2-7M were immobilized by capturing the enzymatically biotinylated proteins onto the surface of sensor chip coated with streptavidin at high (ca. 8000 RU) density.

Figure. 4. Solubility of TGF-β2 and monomeric variants. *A, C*. TGF-β2 and mTGF-β2 (*A*) and mmTGF-β2 and mmTGF-β2-7M (*C*) were diluted from a concentrated stock in 100 mM acetic acid into either PBS

at 7.4 ('Neutral pH') or 100 mM acetic acid ('Acidic pH) and the light scattering at 340 nm was measured. *B, D*. TGF-β2 and mTGF-β2 (*B*) and mmTGF-β2 and mmTGF-β2-7M (*D*) samples diluted into either PBS or 100 mM acetic acid were centrifuged for 5 mins at 20,000 x g and the protein absorbance at 280 nm was measured.

Figure 5. Structure of mmTGF-β2-7M and mmTGF-β2-7M:TβRII complex. *A*. Assigned ^{1}H-^{15}N HSQC spectrum of mmTGF-β2-7M recorded in 10 mM sodium phosphate, 10 mM CHAPS, 5% $^{2}H_2O$, pH 4.70, 37 °C, 800 MHz. Assigned backbone amide signals are indicated by their residue number and one letter amino acid code. *B*. Overlay of 1.8 Å crystal structure of mmTGF-β2-7M (dark red ribbon) with one of the monomers from the 1.8 Å crystal structure of TGF-β2 (PDB 2TGI, blue ribbon). Major structural features are indicated, along with the newly created loop in mmTGF-β2 (red) which takes the place of the heel (α3) helix in TGF-β2. *C*. Overlay of the three mmTGF-β2-7M chains (Chain A, B, and C shown in dark red, green, and orange ribbon, respectively) from the crystallographic asymmetric unit. Dashed line corresponds to missing segments in the newly created loop in Chains A and C due to weak electron density. Other details as in panel *B*. *D*. Overlay of the 1.8 Å crystal structure of mmTGF-β2-7M:TβRII complex (dark red and orange ribbons, respectively) with one of the TGF-β3 monomers and its bound TβRII from the 3.0 Å crystal structure of the TGF-β3:TβRII:TβRI complex (PDB 2PJY, TGF-β3 monomer and TβRII shown in dark blue and cyan ribbon, respectively; TβRI not shown for clarity). Newly created loop in mmTGF-β2 (red) which takes the place of the heel (α3) helix in TGF-β2 is depicted in red. *E*. Overlay as in panel *B*, but expanded to show the near identity of critical hydrophobic and hydrogen-bonding/electrostatic interactions shown previously to be essential for high affinity TGF-β3:TβRII binding (40,41).

Figure 6. Signaling activity of TGF-β dimers and monomers. *A*. TGF-β luciferase reporter activity for TGF-β1, mTGF-β3, and mmTGF-β2-7M shown in solid circles, squares, and triangles, respectively. The solid lines, colored red and blue, correspond to the fitted curves to derive the EC_{50} (green line for mmTGF-β2-7M was not fit due to the lack of signaling activity for this variant). *B*. TGF-β luciferase reporter activity for cells treated with a sub-saturating concentration of TGF-β1 (8 pM) with increasing concentration of the indicated monomeric TGF-β variant added (mTGF-β3 and mmTGF-β2-7M shown in open squares and closed triangles, respectively). The solid blue line corresponds to the fitted curve for mTGF-β3 to derive the EC_{50}. The solid green line corresponds to the fitted curve for mTGF-β2-7M to derive the IC_{50}.

Figure 7. TR-FRET assay for ligand-mediated assembly of TβRI:TβRII complexes. *A*. Structure of the TGF-β3:TβRII:TβRI complex with tags appended to the C-terminus of TβRI and TβRII and fluorescently labeled donor and acceptor proteins that associate with the tags. TβRII has a C-terminal hexahistidine tag (His_6) and is bound by an Tb^{3+}-cryptate labeled antihexahistidine tag antibody (CisBio, Bedford, MA). TβRI has a C-terminal biotinylated avitag and is bound by XL_{665}-labeled streptavidin (CisBio, Bedford, MA). The single lysine residue in TβRI C-terminal avitag that is biotinylated is labeled as "K-B". *B*. Preassembled TGF-β3:TβRII-His (1:2), mTGF-β3:TβRII-His (1:1), and mmTGF-β2-7M:TβRII-His (1:1) complexes at a concentration of 100 nM (blue bars) or 250 nM (grey bars) were incubated with 50 nM biotinylated TβRI-ΔC-Avi and 2 nM Tb-anti-His and 30nM SA-665 for 2 hours at room temperature. Buffer control (orange bars) contained only 2 nM Tb-anti-His and 30nM SA-665. Measurements were performed using a BMG Labtech Pherastar FS. ΔF for each sample was determined by assigning two buffer control assays as the negative control as described in *Experimental Procedures*.

Figure 1

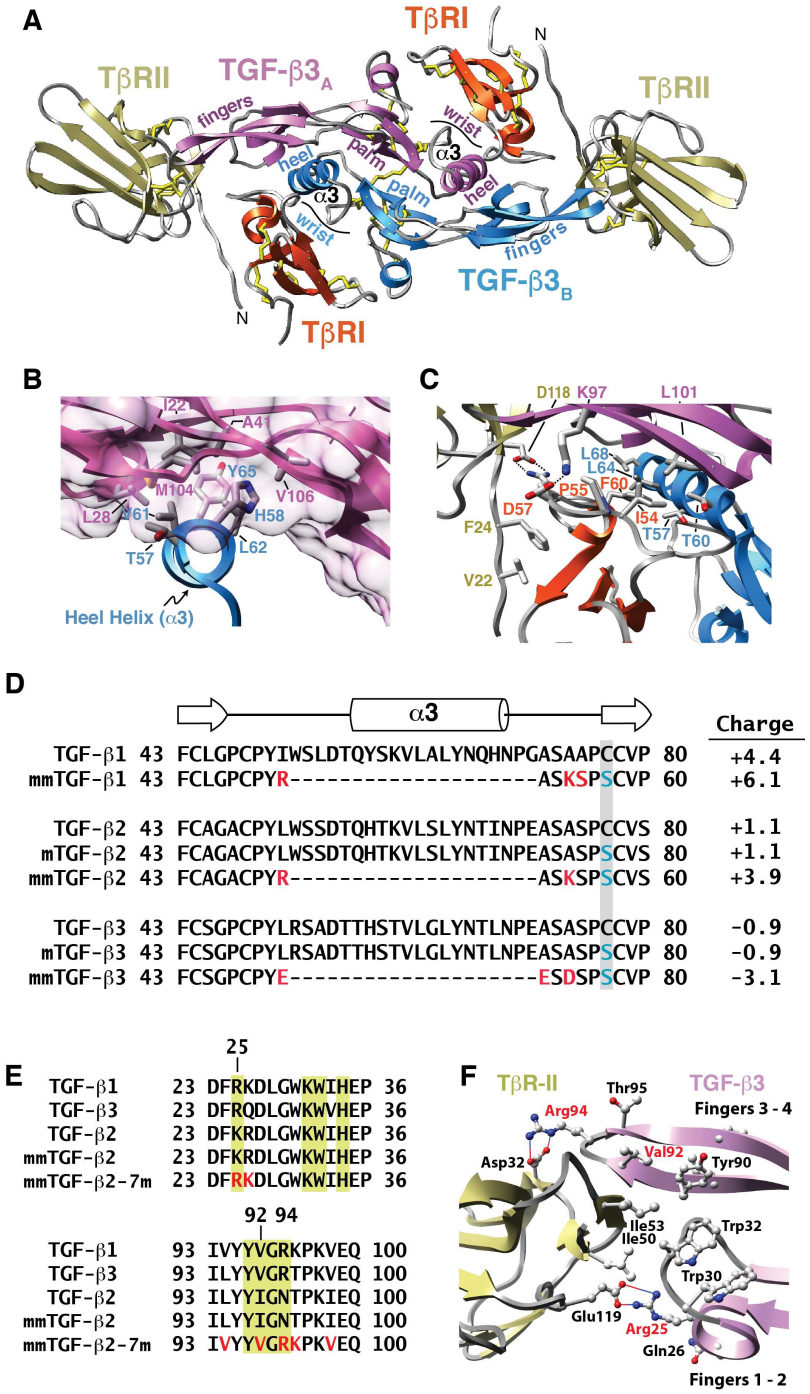

Figure 2

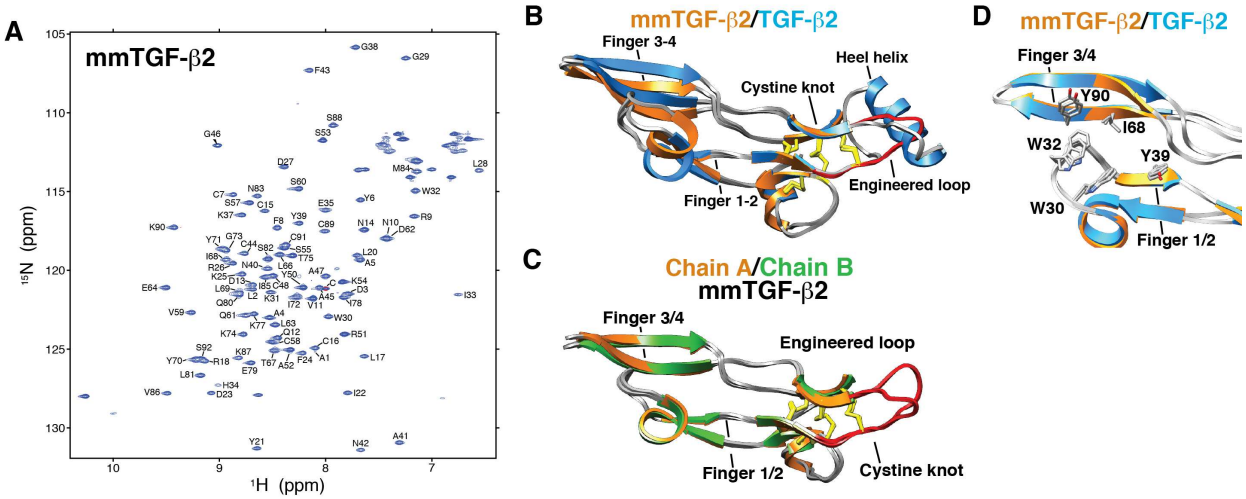

Figure 3

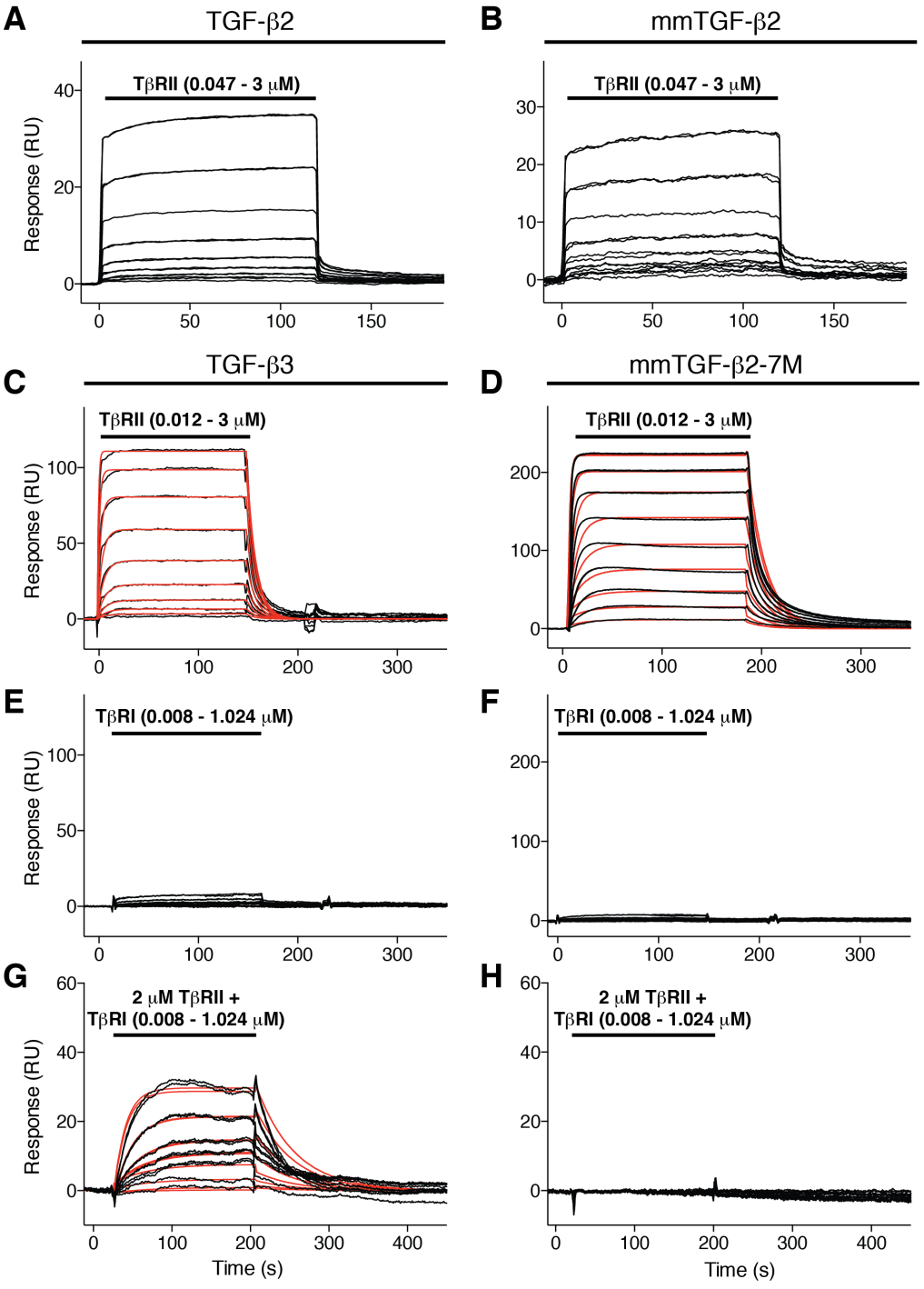

Figure 4

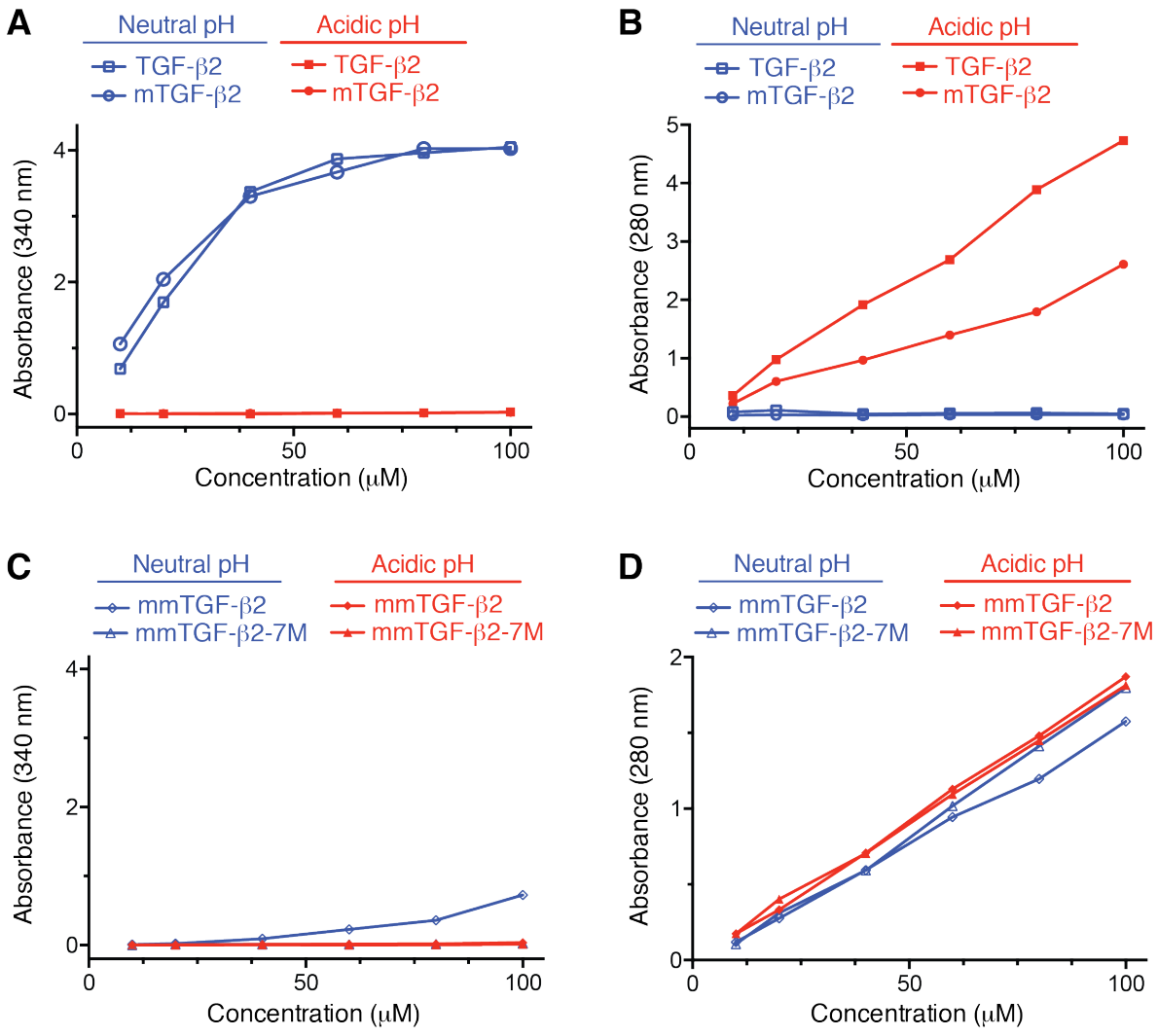

Figure 5

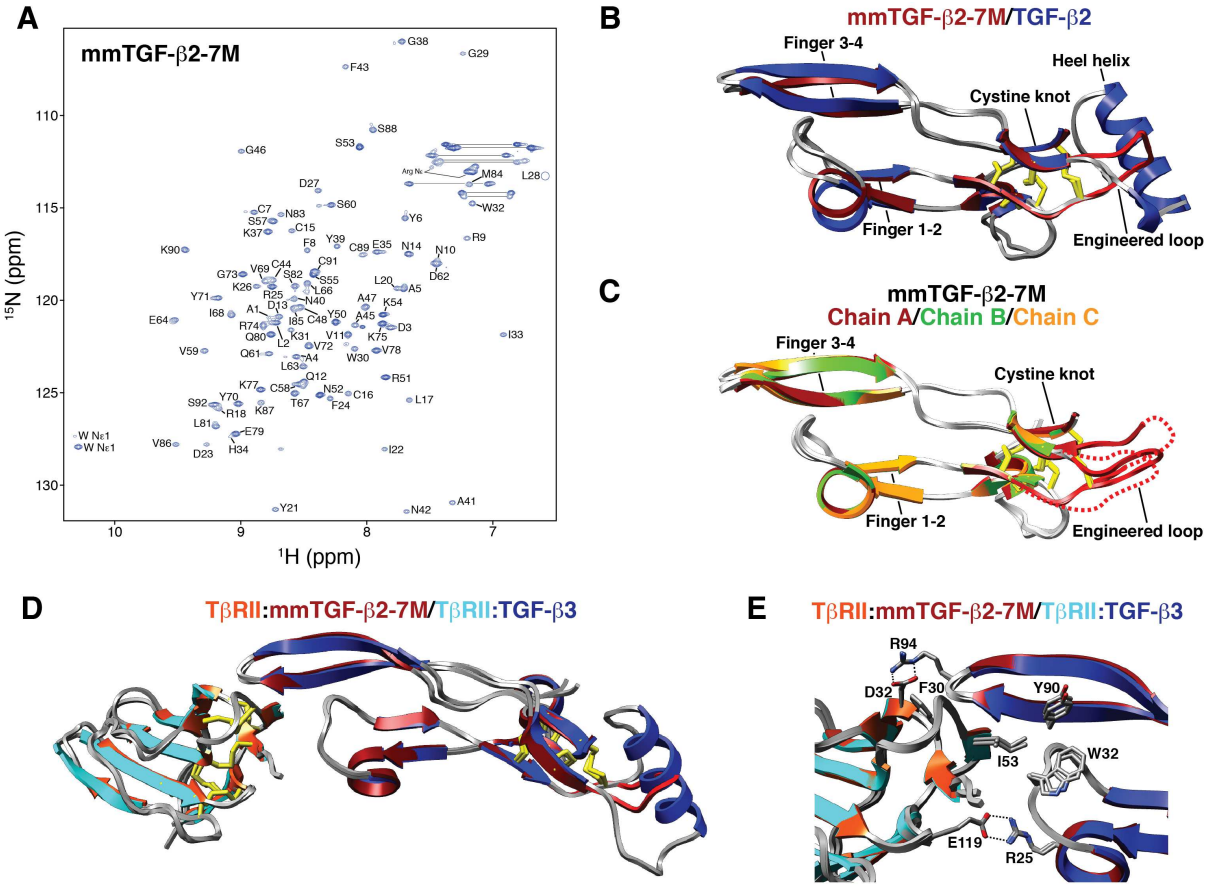

Figure 6

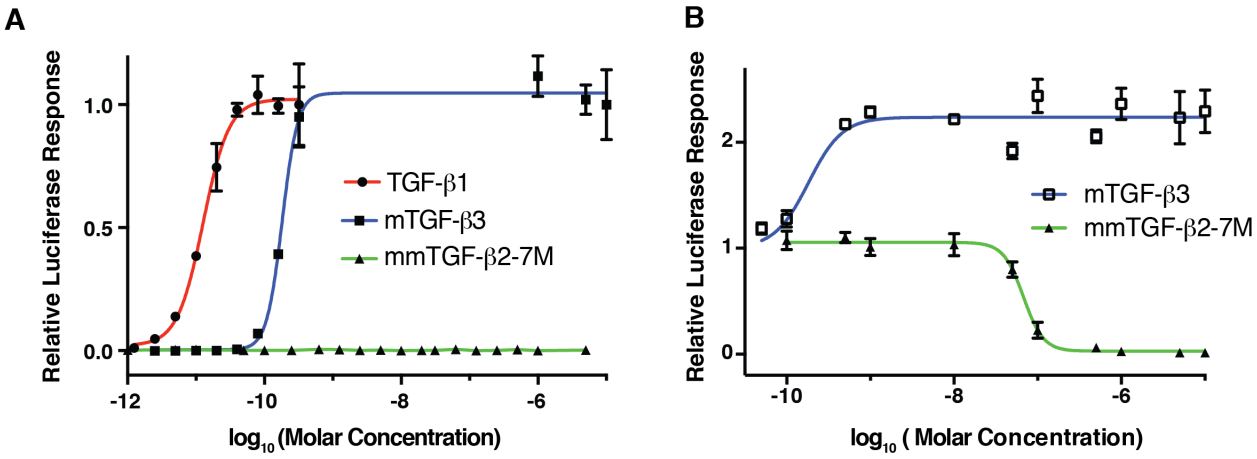

Figure 7

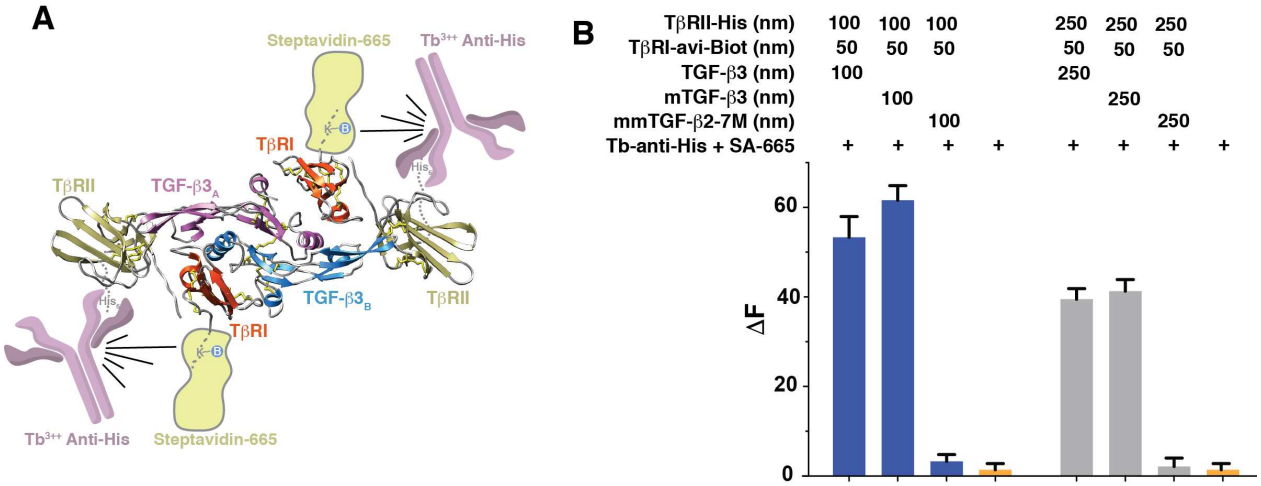

Supplemental Data

An engineered TGF-β monomer that functions as a dominant negative to block TGF-β signaling

Sun Kyung Kim, Lindsey Barron, Cynthia S. Hinck, Elyse M. Petrunak, Kristin E. Cano, Avinash Thangirala, Brian Iskra, Molly Brothers, Machell Vonberg, Belinda Leal, Blair Richter, Ravindra Kodali, Alexander B. Taylor, Shoucheng Du, Christopher O. Barnes, Traian Sulea, Guillermo Calero, P. John Hart, Matthew J. Hart, Borries Demeler, and Andrew P. Hinck

Table S1. TGF-β variants used in this study

Variant Name	Variant Description	Number Residues per Monomer	Single amino acid substitution(s)	Deletion	Tag
TGF-β1	Human TGF-β1 wild type homodimer	112	None	None	None
TGF-β2	Mouse TGF-β2 wild type homodimer	112	None	None	None
TGF-β3	Human TGF-β3 wild type homodimer	112	None	None	None
avi-TGF-β3	Human TGF-β3 wild type homodimer with N-terminal Avitag	127	None	None	N-terminal Avitag
mTGF-β2	Mouse TGF-β2 covalent monomer	112	C77S	None	None
mTGF-β3	Human TGF-β3 covalent monomer	112	C77S	None	None
mmTGF-β1	Human TGF-β1 covalent monomer with α3 replaced with a loop	92	I52R, A74K, A75S C77S	Residues 52-71	None
mmTGF-β2	Mouse TGF-β2 covalent monomer with α3 replaced with a loop	92	L51R, A73K, C77S	Residues 52-71	None
mmTGF-β3	Human TGF-β3 covalent monomer with α3 replaced with a loop	92	L51E, A72E, A74D, C77S	Residues 52-71	None
mmTGF-β2-7M	Mouse TGF-β2 covalent monomer with α3 replaced with a loop	92	K25R, R26K, L51R, A74K, C77S, L89V, I92V, N94R T95K, I98V	Residues 52-71	None
avi-mmTGF-β2-7M	Mouse TGF-β2 covalent monomer with α3 replaced with a loop	107	K25R, R26K, L51R, A74K, C77S, L89V, I92V, N94R T95K, I98V	Residues 52-71	N-terminal Avitag

Figure S1

```
---------- -------MAL DTNYCFSSTE KNCCVRQLYI DFRKDLGWKW   32 TGF-β1
---------- -------MAL DTNYCFSSTE KNCCVRQLYI DFRKDLGWKW   32 mmTGF-β1
---------- -------MAL DAAYCFRNVQ DNCCLRPLYI DFKRDLGWKW   32 TGF-β2
---------- -------MAL DAAYCFRNVQ DNCCLRPLYI DFKRDLGWKW   32 mTGF-β2
---------- -------MAL DAAYCFRNVQ DNCCLRPLYI DFKRDLGWKW   32 mmTGF-β2
---------- -------MAL DAAYCFRNVQ DNCCLRPLYI DFRKDLGWKW   32 mmTGF-β2-7M
MGLNDIFEAQ KIEWHEEFAL DAAYCFRNVQ DNCCLRPLYI DFRKDLGWKW   49 avi-mmTGF-β2-7M
---------- -------MAL DTNYCFRNLE ENCCVRPLYI DFRQDLGWKW   32 TGF-β3
---------- -------MAL DTNYCFRNLE ENCCVRPLYI DFRQDLGWKW   32 mTGF-β3
MGLNDIFEAQ KIEWHEEFAL DTNYCFRNLE ENCCVRPLYI DFRQDLGWKW   49 avi-TGF-β3
---------- -------MAL DTNYCFRNLE ENCCVRPLYI DFRQDLGWKW   32 mmTGF-β3


IHEPKGYHAN FCLGPCPYIW SLDTQYSKVL ALYNQHNPGA SAAPCCVPQA   82 TGF-β1
IHEPKGYHAN FCLGPCPY-- ---------- --------RA SKSPSCVPQA   62 mmTGF-β1
IHEPKGYNAN FCAGACPYLW SSDTQHTKVL SLYNTINPEA SASPCCVSQD   82 TGF-β2
IHEPKGYNAN FCAGACPYLW SSDTQHTKVL SLYNTINPEA SASPSCVSQD   82 mTGF-β2
IHEPKGYNAN FCAGACPY-- ---------- --------RA SKSPSCVSQD   62 mmTGF-β2
IHEPKGYNAN FCAGACPY-- ---------- --------RA SKSPSCVSQD   62 mmTGF-β2-7M
IHEPKGYNAN FCAGACPY-- ---------- --------RA SKSPSCVSQD   79 avi-mmTGF-β2-7M
VHEPKGYYAN FCSGPCPYLR SADTTHSTVL GLYNTLNPEA SASPCCVPQD   82 TGF-β3
VHEPKGYYAN FCSGPCPYLR SADTTHSTVL GLYNTLNPEA SASPSCVPQD   82 mTGF-β3
VHEPKGYYAN FCSGPCPYLR SADTTHSTVL GLYNTLNPEA SASPCCVPQD   99 avi-TGF-β3
VHEPKGYYAN FCSGPCPY-- ---------- --------EE SDSPSCVPQD   62 mmTGF-β3


LEPLPIVYYV GRKPKVEQLS NMIVRSCKCS                        112 TGF-β1
LEPLPIVYYV GRKPKVEQLS NMIVRSCKCS                         92 mmTGF-β1
LEPLTILYYI GNTPKIEQLS NMIVKSCKCS                        112 TGF-β2
LEPLTILYYI GNTPKIEQLS NMIVKSCKCS                        112 mTGF-β2
LEPLTILYYI GNTPKIEQLS NMIVKSCKCS                         92 mmTGF-β2
LEPLTIVYYV GRKPKVEQLS NMIVKSCKCS                         92 mmTGF-β2-7M
LEPLTIVYYV GRKPKVEQLS NMIVKSCKCS                        109 avi-mmTGF-β2-7M
LEPLTILYYV GRTPKVEQLS NMVVKSCKCS                        112 TGF-β3
LEPLTILYYV GRTPKVEQLS NMVVKSCKCS                        112 mTGF-β3
LEPLTILYYV GRTPKVEQLS NMVVKSCKCS                        129 avi-TGF-β3
LEPLTILYYV GRTPKVEQLS NMVVKSCKCS                         92 mmTGF-β3
```

Figure S1. Alignment of the amino acid sequences of the TGF-βs used in this study. Sequences are numbered such that the first residue following the N-terminal methionine is residue 1.

Figure S2

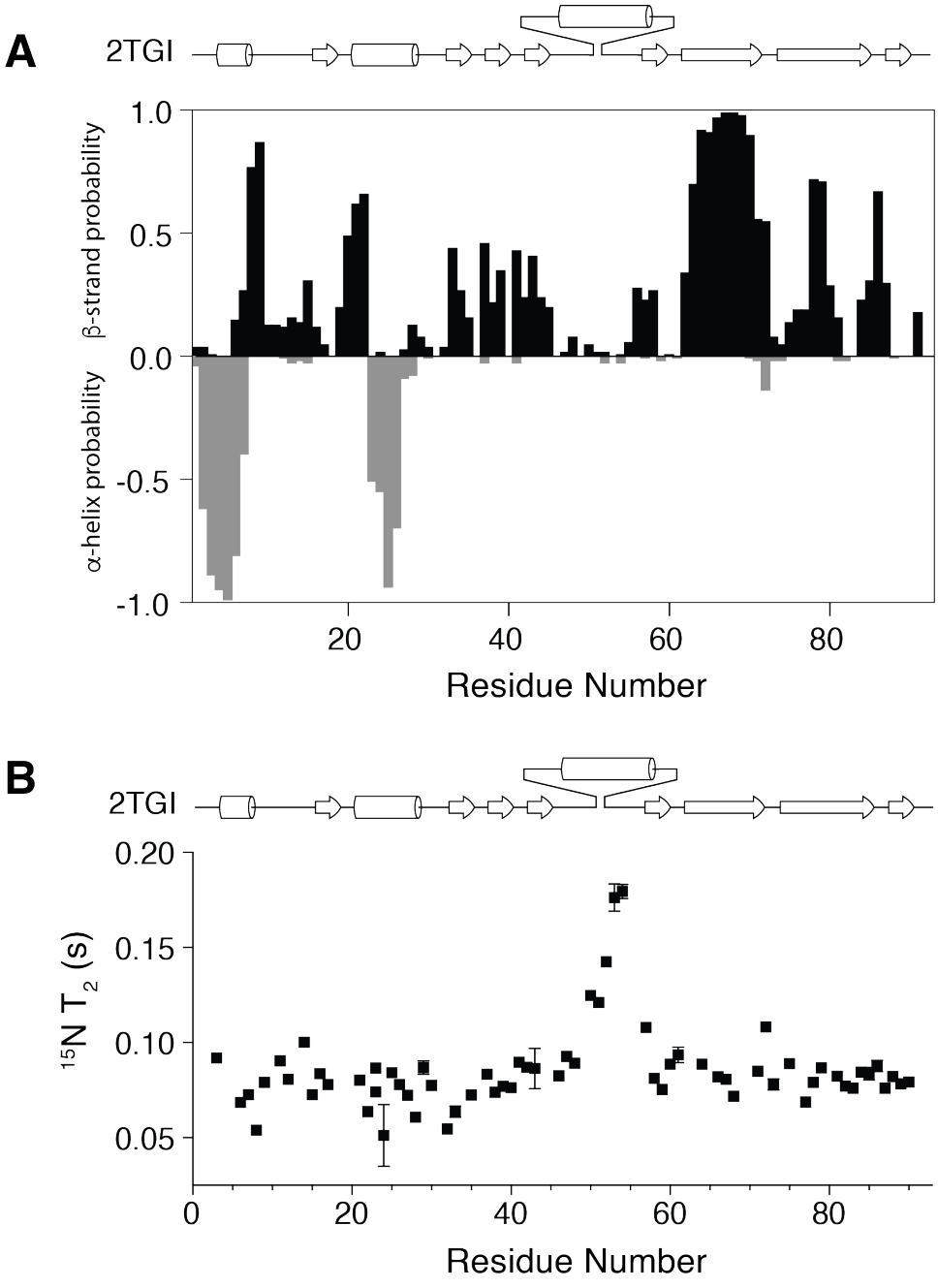

Figure S2. Secondary structure probabilities and backbone ^{15}N T_2 relaxation times for mmTGF-β2. *A*. Secondary structure probabilities were calculated based on the backbone H^N, N^H, Cα, and C^O and sidechain Cβ atoms using the program PECAN. β-strand and α-helix probabilities are plotted as positive and negative values, respectively. *B*. ^{15}N T2 relaxation times plotted as a function of residue number. Secondary structures shown above panels A and B correspond to those from the crystal structure of TGF-β2 (PDB 2TGI).

Figure S3

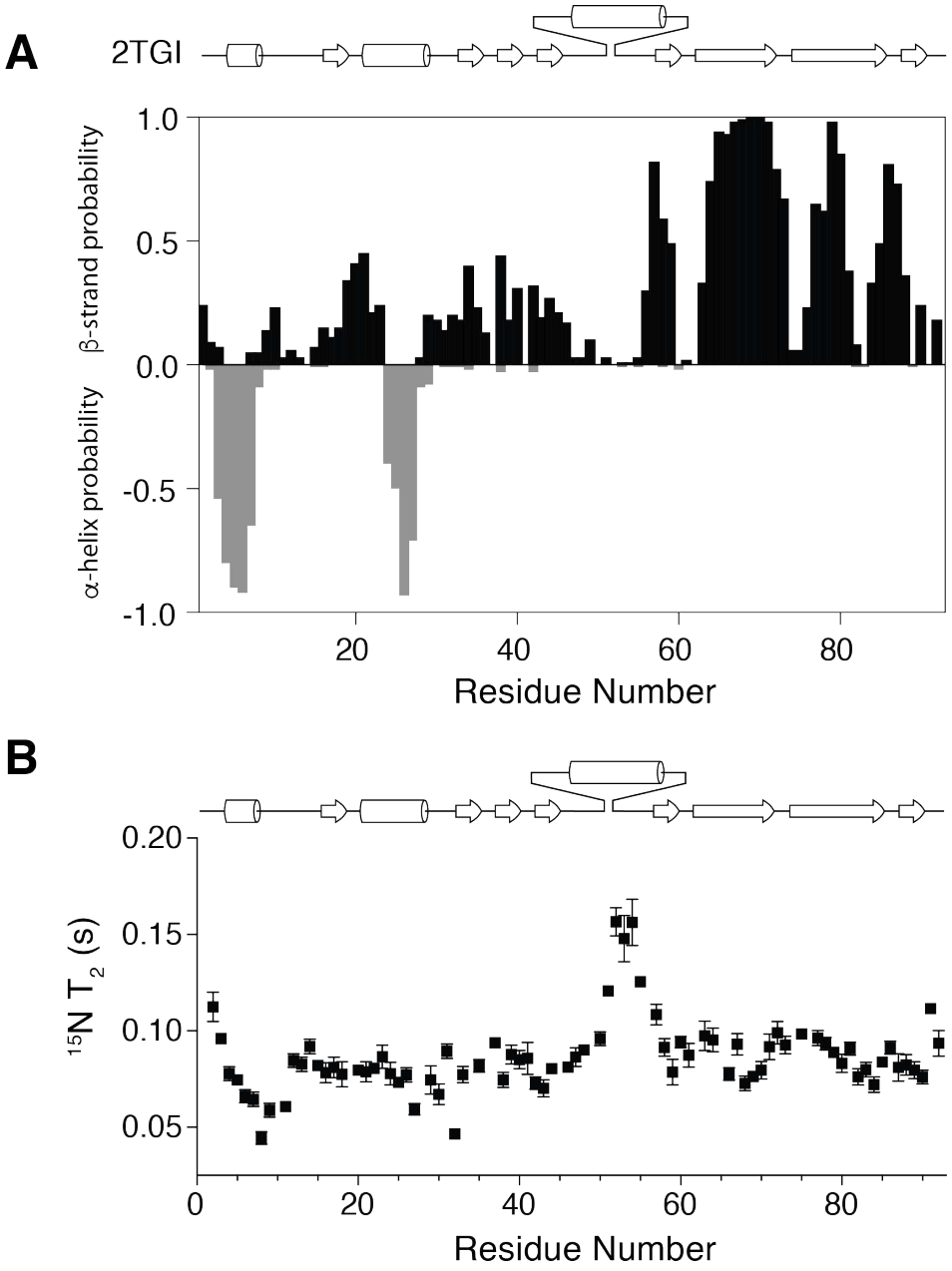

Figure S3. Secondary structure probabilities and backbone ^{15}N T_2 relaxation times for mmTGF-β2-7M. *A*. Secondary structure probabilities were calculated based on the backbone H^N, N^H, Cα, and C^O and sidechain C atoms using the program PECAN. β-strand and α-helix probabilities are plotted as positive and negative values, respectively. *B*. ^{15}N T2 relaxation times plotted as a function of residue number. Secondary structures shown above panels A and B correspond to those from the crystal structure of TGF-β2 (PDB 2TGI).

Figure S4

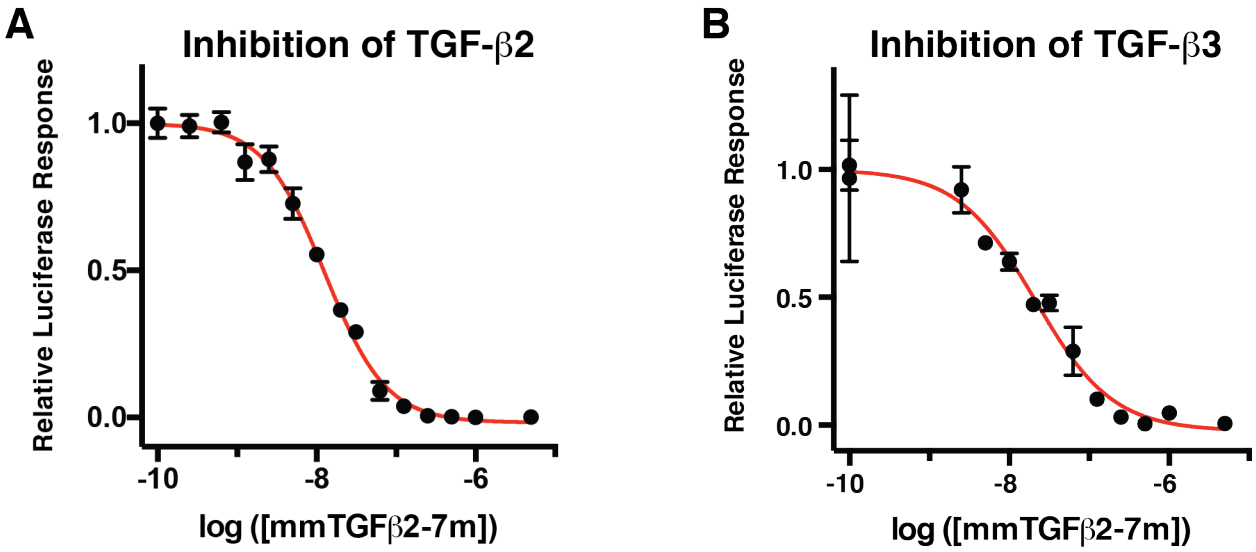

Figure S4. Inhibition of TGF-β2 and TGF-β3 by mmTGF-β2. *A*, *B*. TGF-β luciferase reporter activity for cells treated with a fixed concentration of TGF-β2 (20 pM) (*A*) or TGF-β3 (10 pM) (*B*) and increasing concentrations of mmTGF-β2-7M. Solid red lines correspond to the fitted curve to derive the IC_{50}.

Figure S5

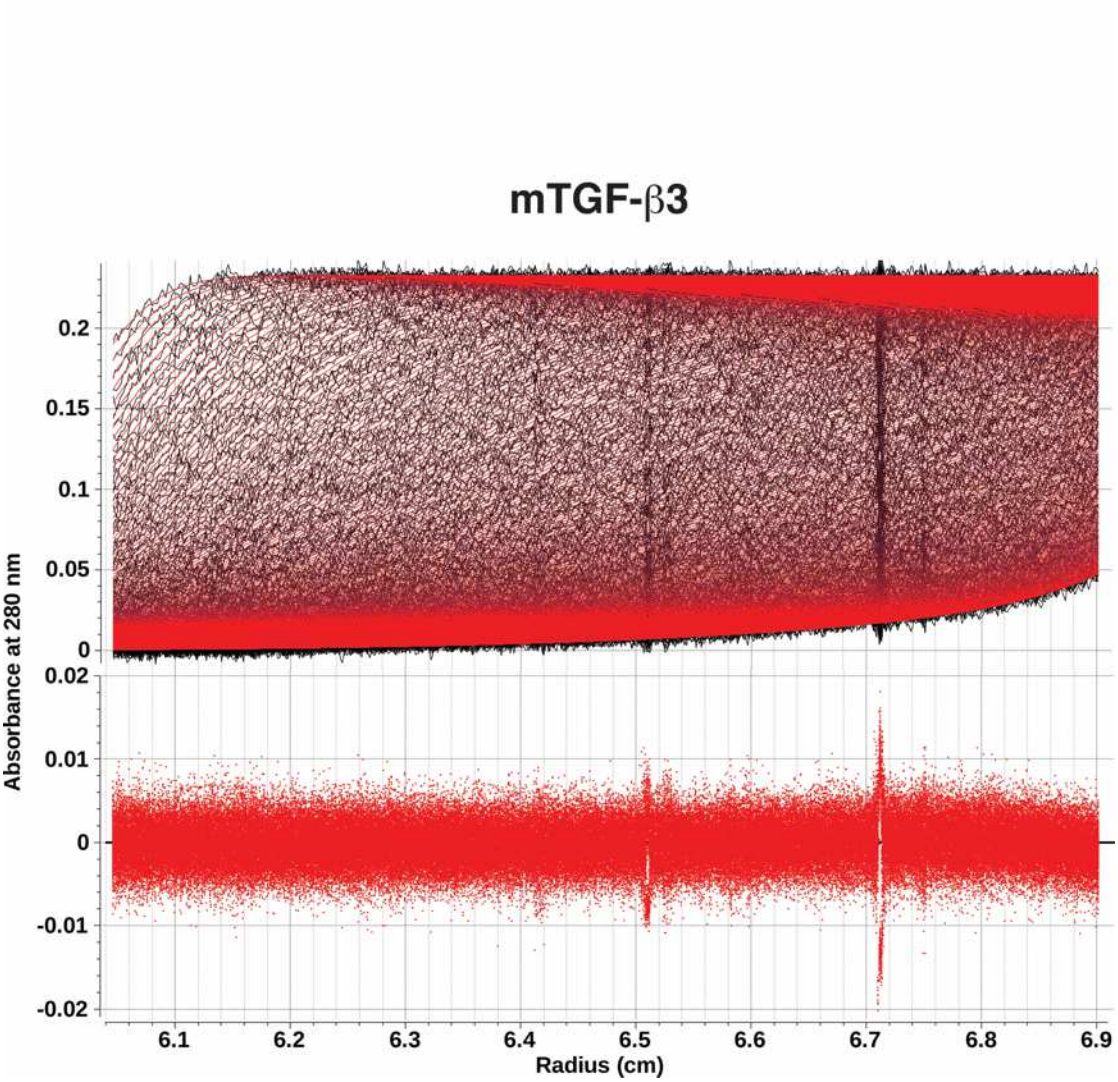

Figure S5. Finite element fit of a reversible monomer-dimer model to the sedimentation velocity experiment of mTGF-β3. Experimental data (black) with finite element fit (red) overlayed shown on top, residuals (red) are shown on the bottom.

Figure S6

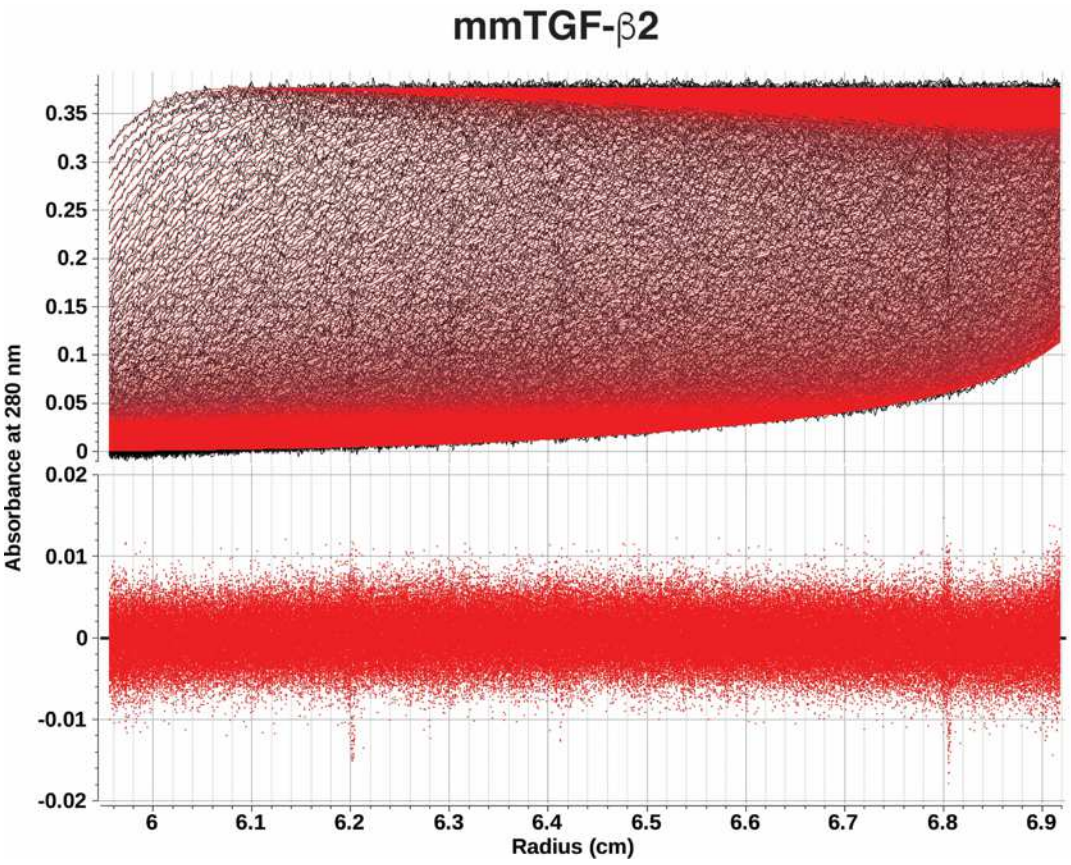

Figure S6. Finite element fit of a reversible monomer-dimer model to the sedimentation velocity experiment of mmTGF-β2. Experimental data (black) with finite element fit (red) overlayed shown on top, residuals (red) are shown on the bottom

Figure S7

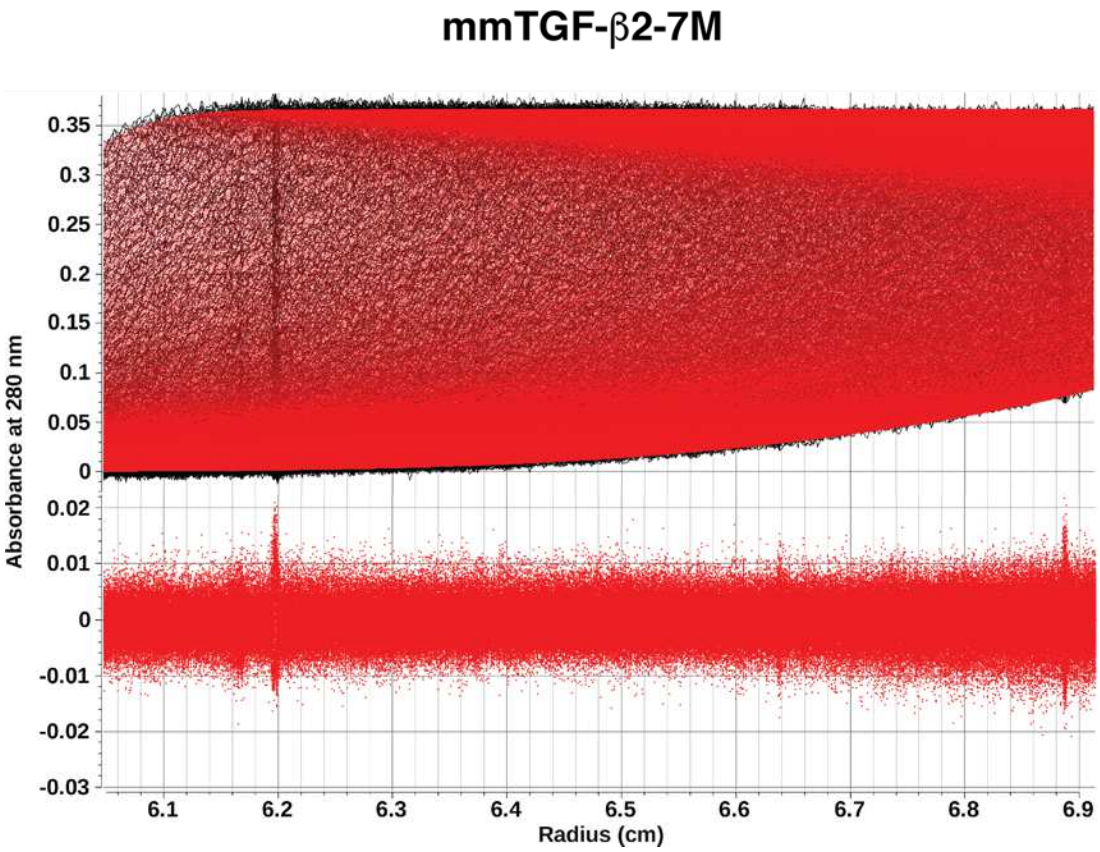

Figure S7. Finite element fit of a reversible monomer-dimer model to the sedimentation velocity experiment of mmTGF-β2-7M. Experimental data (black) with finite element fit (red) overlayed shown on top, residuals (red) are shown on the bottom

Figure S8

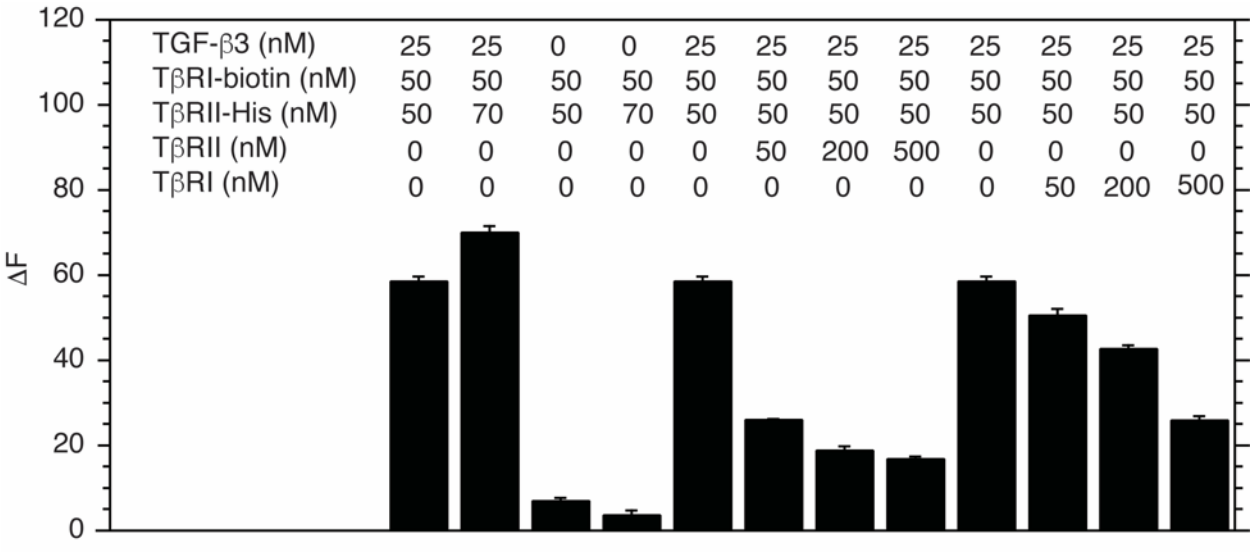

Figure S8. TR-FRET assay for assessing TGF-β:TβRII:TβRI complex assembly. The concentration of the terbium-cryptate anti-hexadhistinde tag antibody donor fluorophore and streptavidin-665 acceptor fluorophore was 2 nM and 30 nM, respectively.

An Engineered TGF-β Monomer that Functions as a Dominant Negative to Block TGF- β Signaling

Sun Kyung Kim, Lindsey Barron, Cynthia S. Hinck, Elyse M. Petrunak, Kristin E. Cano, Avinash Thangirala, Brian Iskra, Molly Brothers, Machell Vonberg, Belinda Leal, Blair Richter, Ravindra Kodali, Alex B. Taylor, Shoucheng Du, Christopher O. Barnes, Traian Sulea, Guillermo Calero, P. John Hart, Matthew J. Hart, Borries Demeler and Andrew P. Hinck

J. Biol. Chem. published online February 22, 2017
